A&A 494, 295–309 (2009)
DOI: 10.1051/0004-6361:200810318
© ESO 2009

Astronomy & Astrophysics

Magnetohydrodynamic waves in a compressible magnetic flux tube with elliptical cross-section

R. Erdélyi and R. J. Morton

Solar Physics and Space Plasma Research Centre (SP^{2}RC), University of Sheffield, Hicks Building, Hounsfield Road, Sheffield S3 7RH, UK
e-mail: [Robertus;app07rjm]@sheffield.ac.uk

Received 3 June 2008 / Accepted 6 November 2008

ABSTRACT

Aims. The propagation of magnetohydrodynamic (MHD) waves in a finite, compressible magnetic flux tube with an elliptical cross-section embedded in a magnetic environment is investigated.
Methods. We present the derivation of the general dispersion relation of linear magneto-acoustic wave propagation for a compressible magnetic flux tube with elliptical cross-section in a plasma with finite beta. The wave modes of propagation for the $n = 0$ (symmetric) sausage and $n = 1$ (anti-symmetric) kink oscillations are then examined within the limit of the thin flux tube approximation.
Results. It is shown that a compressible magnetic tube with elliptical cross-section supports slow and fast magneto-acoustic waves. In the thin tube approximation, the slow sausage mode and the slow and fast kink modes are found in analogue to a circular cross-section. However, the kink modes propagate with different phase speeds depending on whether the axial displacement takes place along the major or minor axis of the ellipse. This feature is present in both the slow and the fast bands, providing two infinite sets of slow kink modes and two infinite sets of fast kink modes, i.e. each corresponding cylindrical mode splits into two sets of modes due to the ellipticity. The difference between the phase speeds along the different axis is dependent on the ratio of the lengths of the two axes. Analytical expressions for the phase speeds are found. We show that the sausage modes do not split due to the introduced ellipticity and only the phase speed is modified when compared to the appropriate cylindrical counterpart. The percentage difference between the periods of the circular and elliptical cross-sections is also calculated, which reaches up to 21% for oscillations along the major axis. The level of difference in period could be very important in magneto-seismological applications, when observed periods are inverted into diagnostic properties (e.g. magnetic field strength, gravitational scale height, tube expansion parameter). Also shown is the perturbation of focal points of the elliptical cross-section for different modes. It is found that the focal points are unperturbed for the sausage mode, but are perturbed for all higher modes.

Key words. magnetohydrodynamics (MHD) – plasmas – Sun: corona – Sun: photosphere – waves

1. Introduction

High resolution imaging and spectroscopic data from the Transitional Region and Coronal Explorer (TRACE) and Solar and Heliospheric Observatory (SOHO) have made it possible to study the plasma fine structure of the solar atmosphere for the first time by observing magnetohydrodynamic (MHD) waves within a variety of open and closed magnetic structures (see Banerjee et al. 2007, for the latest review of observational results with detailed further references therein). The theory of MHD wave propagation in such structures has been developed by first modeling the magnetic structures as homogenous cylindrical magnetic tubes embedded within a magnetic environment (see Edwin & Roberts 1983). The theory was applied to closed structures (e.g. a dense coronal loop with its footpoints anchored in the photosphere) that are able to support standing waves (Roberts et al. 1984).

It was found that the cylindrical flux tube supports an infinite countable set of eigenmodes of slow and fast magneto-acoustic waves which can be split into body and surface waves depending on the spatial behavior of the modes inside the flux tube. There are two characteristic speeds relevant for the propagation of magneto-acoustic waves that have been identified within cylindrical magnetic tubes:

$$c_{\rm T} = \frac{c_{\rm i} v_{\rm Ai}}{\left(c_{\rm i}^2 + v_{\rm Ai}^2\right)^{1/2}}, \qquad c_{\rm k} = \left(\frac{\rho_{\rm i} v_{\rm Ai}^2 + \rho_{\rm e} v_{\rm Ae}^2}{\rho_{\rm i} + \rho_{\rm e}}\right)^{1/2}$$

where $c_{\rm i}$ is the sound speed, $v_{\rm Ai}$ is the Alfvén speed and $\rho_{\rm i}$ is the density of the magnetic tube, whereas $v_{\rm Ae}$ and $\rho_{\rm e}$ are of the magnetic environment. The first speed, which is sub-sonic and sub-Alfvénic, is the tube speed $c_{\rm T}$ of the less dispersive, e.g. sausage, slow mode in the long wavelength approximation under solar conditions. The other characteristic speed is the kink speed $c_{\rm k}$ of the dispersive, e.g. kink, fast mode.

However, actual loops are far more complex than the homogenous cylindrical tube. They are subject to a variety of geometric and physical (often second-order) effects, e.g. stratification, structuring, magnetic twist, curvature, wave leakage, variable background on the time scale of oscillations, etc. to name a few.

Stratification can occur vertically and/or horizontally within the loop. The cause of stratification can be attributed to gravity (e.g. Roberts & Webb 1978; Mendoza-Briceño et al. 2004; Andries et al. 2005a; McEwan et al. 2006; Donnelly et al. 2006;

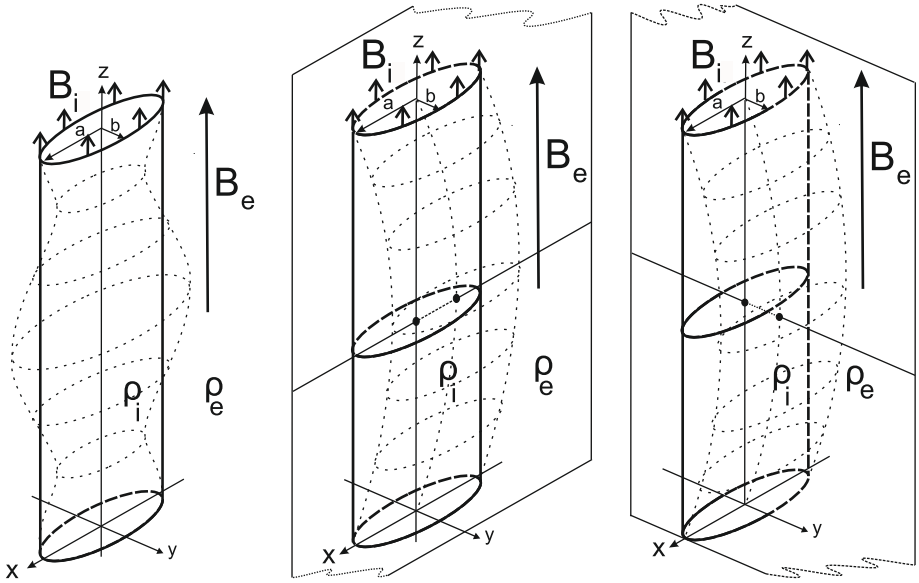

Fig. 1. Sketch showing the equilibrium (bold solid and dashed lines) and perturbed states (thin dashed lines) of a magnetic flux tube with plasma density $\rho_{\rm i}$, magnetic field of strength $\boldsymbol{B}_{\rm i}$ embedded in plasma with density $\rho_{\rm e}$ of strength $\boldsymbol{B}_{\rm e}$. The *left hand sketch* shows the sausage perturbation, the *middle sketch* shows the kink perturbation polarised along the x-axis and the right one shows the kink perturbation polarised along the y-axis. The plane in which the kink modes are polarised is shown.

Díaz & Roberts 2006; Díaz et al. 2007) and density inhomogeneities in the plasma (see, for radial inhomogeneities e.g. Ruderman & Roberts 2002; for longitudinal inhomogeneities e.g. Andries et al. 2005b; Dymova & Ruderman 2006; Erdélyi & Verth 2007; Verth et al. 2007).

Erdélyi & Fedun (2006), Erdélyi & Carter (2006) examined the effect of radial inhomogeneities in the form of structuring by analysing a uniformly twisted magnetic annulus surrounding a straight magnetic core (for a uniformly twisted tube without radial inhomogeneities see Bennett et al. 1999; for weak twist with longitudinal density inhomogeneities see Ruderman 2007). It was found that as the strength of the magnetic twist increased so did the period of the loop, with a greater increase in period for photospheric conditions than coronal conditions. The size of the annulus compared to the magnetic core also affected the size of the period.

The effect of curvature has been examined by Van Doorsselaere et al. (2004) where it was found that the kink mode deviation from the cylindrical frequencies was small.

Damping that will cause complex eigenmodes (or periods) of oscillations is also a factor, however the effect is assumed to be small in the first order approximations of theoretical approaches. Damping can arise from viscous, Ohmic and radiative dissipation (see, e.g. Karami et al. 2002, for viscous and Ohmic dissipation). Further damping mechanisms are resonant absorption and phase mixing, both with their own extensive literature (for list of references see e.g. Aschwanden 2005), which are efficient but in their details still debated. Wave leakage has similar effects to damping and occurs in magnetic tubes when external, laterally non-evanescent magneto-acoustic waves carry away energy from the tube modes. The effects of leaky waves, also referred to as acoustic damping, is first discussed by Cally (1986). The amount of leakage is further aided by the curvature of a loop, with a high degree of curvature causing an increase in the wave leakage. Another possible cause of wave leakage is when photospheric footpoints are not considered a perfect line-tied boundary condition and waves can leak through these boundaries (De Pontieu et al. 2001). For a full discussion on modes of damping see e.g. Roberts (2000); Ruderman (2005).

There is also the theoretical possibility that the geometry of the loop's cross-section is non-circular. In the solar atmosphere, there will be gravitational force acting on the magnetic loops. If the radius of the flux tube is comparable or even just partially comparable to the scale height of gravity, there will then be a vertical distortion of the cross-section for an appropriately tilted flux tube. The distorted flux tube will not then have the rotational symmetry along its axis present otherwise in the cylindrical case. Ellipticity could also be due to the curvature of the tube. At the photospheric level, the flux tubes are mainly vertical and gravity would effect the shape of the cross-section to a lesser extent. However, intense flux tubes located at the supergranule boundaries could still have a non-circular, strongly elongated cross-section due to horizontal motions of the convective cells distorting the tube cross-section. Observations from the Swedish Solar Telescope show evidence of distortion at photospheric level. The study of magnetic bright points believed to occur at the footpoints of coronal loops, highlight the tube cross-section. The cross-sections observed have highly distorted shape. To the best of our knowledge, currently there is no observational study that investigates the shape of cross-sections of magnetic flux tubes present in the photosphere and corona. The lack of such studies is most probably due to limited spatial resolution. With this work here, we wish to contribute to the theoretical foundation of MHD wave studies in flux tubes with non-cylindrical cross-sections.

In this paper the propagation of magneto-acoustic waves within a straight magnetic tube with an elliptical cross-section is considered. The elliptical cross-section is the simplest distortion from rotational symmetry. The tube is embedded within a magnetic environment and both internal and external plasmas have a finite plasma beta, i.e. the magnetised plasma is compressible with non-zero temperature. The analysis follows on from Ruderman (2003) who investigated a magnetic tube with an elliptical cross-section in a zero beta plasma, however, the effects of damping will not be addressed here. For the sake of simplicity

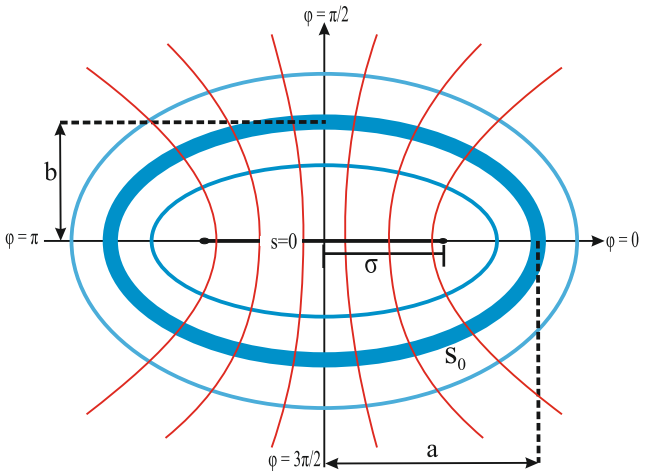

Fig. 2. A sketch of elliptical coordinates in the xy plane. The elliptical coordinates are (s, φ). The curves of s = constant are the confocal ellipses and curves of φ = constant are the orthogonal hyperbolae. The thick confocal ellipse represents the boundary of the tube, $s = s_0$. σ is the distance between the center of the ellipse and the focal points.

the explicit effects of e.g. gravity or granular shear, on the shaping of the cross-section is ignored and we concentrate on the elliptical structure outlined by the magnetic field within a uniform medium. In particular, we will search for solutions of the linear governing equations that provide a model for wave propagation for typical photospheric and coronal conditions. However, as discussed previously (Edwin & Roberts 1983), we acknowledge that gravitational effects are important in the photosphere and caution should be exercised when applying the results for the flux tube oscillations in the lower part of the solar atmosphere.

The cylindrical geometry is a special case of the elliptical problem, so it is expected to recover many of the modes that are found in Edwin & Roberts (1983) with some new features arising from the difference in length of the major and minor axis of the ellipse. This expectation is already confirmed to some extent for zero beta plasma by Ruderman (2003).

We present the derivation of a more general dispersion relation allowing full compressibility for an elliptical magnetic flux tube, followed by analysis of the approximate behavior in the case of the thin tube approximation, i.e. when the width of the flux tube is small compared to the wavelengths and length of the loop. Here it is shown, that (i) in spite of the elliptical structure, there is only change to the phase speed of the sausage mode and its higher harmonics in the slow and fast bands compared to the cylindrical analogues; (ii) that there are two infinite sequences of magneto-acoustic tube eigenmodes, $\omega_{n\mathrm{M}}$ and $\omega_{n\mathrm{m}}$ $(n = 1, 2, ...)$. The eigenfrequencies $\omega_{1\mathrm{M,m}}$ correspond to two kink modes, where $\omega_{1\mathrm{M}}$ is polarised along the major axis and $\omega_{1\mathrm{m}}$ is polarised along the minor axis of the elliptical cross-section. A comparison between the frequencies of the elliptical and cylindrical geometries is then performed for different values of ellipticity, where we analyse the effect of ellipticity on the period of the magnetic flux tube in order to serve impetus for magneto-seismological applications.

2. General dispersion relation

Consider a magnetic flux tube with an elliptical cross-section embedded vertically in a homogenous, ideal plasma. The magnetic field inside is uniform and of the form $\boldsymbol{B}_\mathrm{i} = B_\mathrm{i}\hat{\boldsymbol{z}}$, with the external magnetic field $\boldsymbol{B}_\mathrm{e} = B_\mathrm{e}\hat{\boldsymbol{z}}$. Here, $\hat{\boldsymbol{z}}$ is the unit vector in the z-direction. Linear perturbations about the equilibrium are described by the linear, ideal MHD equations

$$\frac{\partial \rho_1}{\partial t} = -\nabla.(\rho \boldsymbol{v}), \qquad \rho\frac{\partial \boldsymbol{v}}{\partial t} = -\nabla p_1 + \frac{1}{\mu_0}(\nabla \times \boldsymbol{b}) \times \boldsymbol{B}, \tag{1}$$

$$\frac{\partial \boldsymbol{b}}{\partial t} = \nabla \times (\boldsymbol{v} \times \boldsymbol{B}), \qquad \frac{\partial p_1}{\partial t} = c_\mathrm{s}^2\left(\frac{\partial \rho_1}{\partial t} + (\boldsymbol{v}.\nabla)\rho\right) - (\boldsymbol{v}.\nabla)p.$$

Here ρ is the equilibrium density, p is the equilibrium pressure, $\boldsymbol{v}$ is the velocity perturbation, $\boldsymbol{b}$ is the perturbation of the magnetic field, p_1 is the pressure perturbation, ρ_1 is the density perturbation, c_s is the sound speed and μ_0 is the magnetic permeability of free space.

The equations in (1) can be combined to obtain (see, for example Lighthill 1960)

$$\frac{\partial^2}{\partial t^2}\left(\frac{\partial^2}{\partial t^2} - \left(c_\mathrm{s}^2 + v_\mathrm{A}^2\right)\nabla^2\right)(\nabla.\boldsymbol{v}) + c_\mathrm{s}^2 v_\mathrm{A}^2\frac{\partial^2}{\partial z^2}\nabla^2(\nabla.\boldsymbol{v}) = 0, \tag{2}$$

where v_A is the Alfvén speed.

Let us introduce elliptical coordinates which are related to the Cartesian coordinates via

$$x = \sigma\cosh s\cos\varphi, \qquad y = \sigma\sinh s\sin\varphi, \tag{3}$$

where s and φ are the elliptical coordinates, σ is the characteristic value of length and is also the x-coordinate of the focal points, i.e. the focal points are situated at $(x, y) = (\pm\sigma, 0)$. Let the flux tube boundary with elliptical cross-section be at $s = s_0$, so the tube cross-section has a major axis a and a minor axis b given by

$$a = \sigma\cosh(s_0), \qquad b = \sigma\sinh(s_0). \tag{4}$$

The eccentricity of the tube cross-section is

$$\epsilon = \left(1 - \frac{b^2}{a^2}\right)^{1/2} = \frac{1}{\cosh(s_0)}.$$

As eccentricity tends to zero the cross-section can be approximated by a circle. The Laplacian operator in elliptical coordinates (Korn & Korn 1961) is given by

$$\nabla^2 = H^{-2}\left(\frac{\partial^2}{\partial s^2} + \frac{\partial^2}{\partial \varphi^2}\right) + \frac{\partial^2}{\partial z^2},$$

where $H^2 = \sigma^2(\sinh^2 s + \sin^2\varphi)$.

The condition of pressure balance implies

$$p_\mathrm{i} + P_\mathrm{i} = p_\mathrm{e} + P_\mathrm{e}, \tag{5}$$

where

$$P = \frac{B^2}{2\mu_0}$$

is the magnetic pressure. Since the equilibrium quantities depend only on s and φ, the perturbed quantities can be Fourier-analysed with respect to t and z. We can then write

$$\Delta = \nabla.\boldsymbol{v} \propto S(s)\Phi(\varphi)\exp(\mathrm{i}(kz - \omega t)), \tag{6}$$

where $S(s)$ and $\Phi(\varphi)$ are functions to be determined and k is the wavenumber in the z direction. Substituting (6) into (2) and after some simple algebra one obtains for the internal region

$$H^{-2}\left(\frac{1}{S}\frac{\partial^2 S}{\partial s^2} + \frac{1}{\Phi}\frac{\partial^2 \Phi}{\partial \varphi^2}\right) + \frac{4}{\sigma^2}m_\mathrm{i}^2 = 0, \tag{7}$$

where

$$m_{\rm i}^2 = \frac{\sigma^2}{4}\frac{\left(\omega^2-\omega_{\rm i}^2\right)\left(\omega^2-\omega_{\rm Ai}^2\right)}{\left(c_i^2+v_{\rm Ai}^2\right)\left(\omega^2-\omega_{\rm T}^2\right)}, \qquad \omega_{\rm T} = \frac{c_i\omega_{\rm Ai}}{\left(c_i^2+v_{\rm Ai}^2\right)^{1/2}},$$

$$\omega_{\rm i} = kc_{\rm i}, \qquad \omega_{\rm A} = kv_{\rm Ai}.$$

Here $m_{\rm i}^2$ may be positive or negative, where $m_{\rm i}^2 > 0$ corresponds to spatially oscillating body waves and $m_{\rm i}^2 < 0$ corresponds to evanescent surface waves. Let us now write (7) in the form

$$\frac{1}{S}\frac{\partial^2 S}{\partial s^2} + 4m_{\rm i}^2\sinh^2 s = -\left(\frac{1}{\Phi}\frac{\partial^2\Phi}{\partial\varphi^2} + 4m_{\rm i}^2\sin^2\varphi\right). \tag{8}$$

It can be seen that the left hand side depends only upon s and the right only upon φ. Each side is therefore equal to a constant, hence there are two separate equations given by

$$\frac{\partial^2\Phi}{\partial\varphi^2} + \left(h - 2m_{\rm i}^2\cos 2\varphi\right)\Phi = 0, \tag{9}$$

and

$$\frac{\partial^2 S}{\partial s^2} - \left(h - 2m_{\rm i}^2\cosh 2s\right)S = 0, \tag{10}$$

where h is the constant to be determined. Equation (9) is known as the Mathieu equation and (10) is the modified Mathieu equation (see Abramowitz & Stegun 1964; Arscott 1964). The Mathieu equation has even solutions of the form $\Phi = {\rm ce}_n\left(\varphi, m_{\rm i}^2\right)$, where ${\rm ce}_n\left(\varphi, m_{\rm i}^2\right)$ is an even function with n zeros in the interval $0 \le \varphi \le \pi$. The odd solutions are given by $\Phi = {\rm se}_n\left(\varphi, m_{\rm i}^2\right)$, where ${\rm se}_n\left(\varphi, m_{\rm i}^2\right)$ is an odd function with n zeros in the interval $0 \le \varphi \le \pi$. The functions ${\rm ce}_n\left(\varphi, m_{\rm i}^2\right)$ and ${\rm se}_n\left(\varphi, m_{\rm i}^2\right)$ are the Mathieu functions, also referred to as the angular Mathieu functions in applications involving elliptical coordinates. The solution can either be even or odd but not both. The modified Mathieu equation solutions are given by the modified Mathieu functions $S = {\rm Ce}_n(s, m_{\rm i}^2)$ (even) and $S = {\rm Se}_n(s, m_{\rm i}^2)$ (odd), also referred to as the radial Mathieu functions in applications involving elliptical coordinates. For a visual introduction into the properties of both the Mathieu and modified Mathieu functions see, e.g. Gutiérrez-Vega et al. (2003).

The solutions to Eqs. (9) and (10) also have to satisfy the regularity conditions:

$$P_{\rm T,1}(s,\varphi) = P_{\rm T,1}(s,-\varphi), \qquad v_{\rm s}(s,\varphi) = -v_{\rm s}(s,-\varphi) \tag{11}$$

at $s = 0$. Here, $P_{\rm T,1} = p_1 + P_1$ is the total pressure perturbation inside the tube and $v_{\rm s}$ is the velocity in the s direction. These conditions arise because the points $(s = 0, \varphi_0)$ and $(s = 0, -\varphi_0)$ are the same point in the xy plane.

Equations (1) can be written in terms of $\nabla.\boldsymbol{v}$, then substituting in (6) gives

$$\hat{v}_{\rm s}(s,\varphi) = -\frac{\left(\omega^2-\omega_{\rm i}^2\right)}{H\omega^2 m_{\rm i}^2}\frac{\partial S(s)}{\partial s}\Phi(\varphi),$$

$$\hat{v}_{\varphi}(s,\varphi) = -\frac{\left(\omega^2-\omega_{\rm i}^2\right)}{H\omega^2 m_{\rm i}^2}S(s)\frac{\partial\Phi(\varphi)}{\partial\varphi},$$

$$\hat{v}_z(s,\varphi) = -\frac{{\rm i}kc_i^2}{\omega^2}S(s)\Phi(\varphi),$$

$$\hat{b}_z(s,\varphi) = -{\rm i}B_{\rm i}\frac{\omega^2-\omega_{\rm i}^2}{\omega^3}S(s)\Phi(\varphi),$$

$$\hat{p}_1(s,\varphi) = -{\rm i}\rho_{\rm i}\frac{c_i^2}{\omega}S(s)\Phi(\varphi),$$

$$\hat{P}_{\rm T,1}(s,\varphi) = -\frac{\rm i}{\omega^3}\left[B_{\rm i}^2\left(\omega^2-\omega_{\rm i}^2\right) + \omega^2 c_i^2\rho_{\rm i}\right]S(s)\Phi(\varphi), \tag{12}$$

inside the tube, where the hat notation denotes the (s,φ) dependent parts of the perturbations. It can be seen from (12), when $\Phi = {\rm ce}_n\left(\varphi, m_{\rm i}^2\right)$ the first condition of (11) is satisfied. The second condition gives $S'(0)\Phi(\varphi) = -S'(0)\Phi(\varphi)$, i.e $S'(0) = 0$, where the prime indicates the derivative with respect to s. The only solution of (10) is then ${\rm Ce}_n(s, m_{\rm i}^2)$ multiplied by some constant. When $\Phi = {\rm se}_n\left(\varphi, m_{\rm i}^2\right)$, the second condition (11) is satisfied and the first condition gives $S(0) = 0$. This time the only solution of (10) is ${\rm Se}_n(s, m_{\rm i}^2)$, again multiplied by some constant. Note that the Mathieu functions can be related to the modified Mathieu functions via

$${\rm Ce}_n\left(s, m_{\rm i}^2\right) = {\rm ce}_n\left({\rm i}s, m_{\rm i}^2\right), \qquad {\rm Se}_n\left(s, m_{\rm i}^2\right) = -{\rm ise}_n\left({\rm i}s, m_{\rm i}^2\right). \tag{13}$$

2.1. Body waves ($m_{\rm i}^2 > 0$)

The general solution to (8), valid for body waves is then

$$\hat{\Delta}_{\rm i} = S(s)\Phi(\varphi) = \alpha_0^i{\rm Ce}_0(s, m_{\rm i}^2){\rm ce}_0\left(\varphi, m_{\rm i}^2\right)$$

$$+\sum_{n=1}^{\infty}\left[\alpha_n^i{\rm Ce}_n\left(s, m_{\rm i}^2\right){\rm ce}_n\left(\varphi, m_{\rm i}^2\right) + \beta_n^i{\rm Se}_n\left(s, m_{\rm i}^2\right){\rm se}_n\left(\varphi, m_{\rm i}^2\right)\right] \tag{14}$$

where α_n^i and β_n^i are arbitrary constants. The general solution can be obtained for the external region in the same way, substituting $m_{\rm e}^2$ for $m_{\rm i}^2$, where

$$m_{\rm e}^2 = \frac{\sigma^2}{4}\frac{(\omega^2-\omega_{\rm e}^2)\left(\omega^2-\omega_{\rm Ae}^2\right)}{\left(c_{\rm e}^2+v_{\rm Ae}^2\right)(\omega^2-\omega_{\rm Te}^2)},$$

$$\omega_{\rm Te} = \frac{c_{\rm e}\omega_{\rm Ae}}{\left(c_{\rm e}^2+v_{\rm Ae}^2\right)^{1/2}}, \qquad \omega_{\rm e} = kc_{\rm e}, \qquad \omega_{\rm Ae} = kv_{\rm Ae}.$$

However, we require that the perturbations are laterally evanescent in the external plasma, i.e. vanish far away from the boundary of the ellipse. We assume $m_{\rm e}^2 < 0$ as this corresponds to the evanescent waves. If $m_{\rm e}^2 > 0$, then the tube may act as a radiator of waves (see Roberts & Webb 1979; Cally 1986; Ruderman & Roberts 2005 for discussion in cylindrical geometry). The general solution to (8) which satisfies the condition of evanescence is

$$\hat{\Delta}_{\rm e} = \alpha_0^{\rm e}{\rm Fek}_0(s, n_{\rm e}^2){\rm ce}_0\left(\varphi, n_{\rm e}^2\right)$$

$$+\sum_{n=1}^{\infty}\left[\alpha_n^{\rm e}{\rm Fek}_n\left(s, n_{\rm e}^2\right){\rm ce}_n\left(\varphi, n_{\rm e}^2\right) + \beta_n^{\rm e}{\rm Gek}_n\left(s, n_{\rm e}^2\right){\rm se}_n\left(\varphi, n_{\rm e}^2\right)\right] \tag{15}$$

where $m_{\rm e}^2 = -n_{\rm e}^2 > 0$. We have also introduced the modified Mathieu functions of the third kind ${\rm Fek}(s, n_{\rm e}^2)$ and ${\rm Gek}(s, n_{\rm e}^2)$ (Arscott 1964) and arbitrary constants $\alpha_n^{\rm e}$ and $\beta_n^{\rm e}$.

Relating the obtained internal and external solutions by requiring that $\hat{v}_{\rm s}$ and $\hat{P}_{\rm T,1}$ are continuous across $s = s_0$ (see

Appendix A), substituting in Eqs. (A.3) and (A.4) and separating the odd and even solutions gives the infinite system of linear homogeneous algebraic equations with respect to $\alpha_n^{\mathrm{i,e}}$ and $\beta_n^{\mathrm{i,e}}$:

$$\frac{\left(\omega^2-\omega_{\mathrm{i}}^2\right)}{2m_{\mathrm{i}}^2}\sum_{q=0}^{\infty}\alpha^{j}_{2q+j}\mathrm{Ce}'_{2q+j}\left(s_0,m_{\mathrm{i}}^2\right)A^{2q+j}_{2r+j}\left(m_{\mathrm{i}}^2\right)=$$

$$\frac{\left(\omega^2-\omega_{\mathrm{e}}^2\right)}{2n_{\mathrm{e}}^2}\sum_{q=0}^{\infty}\alpha^{\mathrm{e}}_{2q+j}\mathrm{Fek}'_{2q+j}\left(s_0,n_{\mathrm{e}}^2\right)A^{2q+j}_{2r+j}\left(n_{\mathrm{e}}^2\right), \tag{16}$$

$$\rho_{\mathrm{i}}\left(c_i^2+v_{\mathrm{Ai}}^2\right)\left(\omega_{\mathrm{T}}^2-\omega^2\right)\sum_{q=0}^{\infty}\alpha^{i}_{2q+j}\mathrm{Ce}_{2q+j}\left(s_0,m_{\mathrm{i}}^2\right)A^{2q+j}_{2r+j}\left(m_{\mathrm{i}}^2\right)=$$

$$\rho_{\mathrm{e}}\left(c_{\mathrm{e}}^2+v_{\mathrm{Ae}}^2\right)\left(\omega_{\mathrm{Te}}^2-\omega^2\right)\sum_{q=0}^{\infty}\alpha^{\mathrm{e}}_{2q+j}\mathrm{Fek}_{2q+j}\left(s_0,n_{\mathrm{e}}^2\right)A^{2q+j}_{2r+j}\left(n_{\mathrm{e}}^2\right) \tag{17}$$

and

$$\frac{\left(\omega^2-\omega_{i}^2\right)}{2m_{\mathrm{i}}^2}\sum_{q=0}^{\infty}\beta^{i}_{2q+1+j}\mathrm{Se}'_{2q+1+j}\left(s_0,m_{\mathrm{i}}^2\right)B^{2q+1+j}_{2r+1+j}\left(m_{\mathrm{i}}^2\right)=$$

$$\frac{\left(\omega^2-\omega_{\mathrm{e}}^2\right)}{2n_{\mathrm{e}}^2}\sum_{q=0}^{\infty}\beta^{\mathrm{e}}_{2q+1+j}\mathrm{Gek}'_{2q+1+j}\left(s_0,n_{\mathrm{e}}^2\right)B^{2q+1+j}_{2r+1+j}\left(n_{\mathrm{e}}^2\right), \tag{18}$$

$$\rho_{\mathrm{i}}\left(c_i^2+v_{\mathrm{Ai}}^2\right)\left(\omega_{\mathrm{T}}^2-\omega^2\right)\sum_{q=0}^{\infty}\beta^{i}_{2q+1+j}\mathrm{Se}_{2q+1+j}\left(s_0,m_{\mathrm{i}}^2\right)B^{2q+1+j}_{2r+1+j}\left(m_{\mathrm{i}}^2\right)=$$

$$\rho_{\mathrm{e}}\left(c_{\mathrm{e}}^2+v_{\mathrm{Ae}}^2\right)\left(\omega_{\mathrm{Te}}^2-\omega^2\right)\sum_{q=0}^{\infty}\beta^{\mathrm{e}}_{2q+1+j}$$

$$\times\mathrm{Gek}_{2q+1+j}\left(s_0,n_{\mathrm{e}}^2\right)B^{2q+1+j}_{2r+1+j}\left(n_{\mathrm{e}}^2\right) \tag{19}$$

where $r=0,1,2...$ Each pair of Eqs. (16), (17) and (18), (19) consists of four equations, two for $j=0$ and two for $j=1$. The condition of existence of non-trivial solutions is that the corresponding infinite determinant of each system is equal to zero. This condition then gives dispersion relations.

Taking the cold plasma case ($c_{\mathrm{i}}=c_{\mathrm{e}}=0$), we recover the equations (see Appendix A) found by Ruderman (2003).

2.2. Surface waves ($m_{\mathrm{i}}^2=-n_{\mathrm{i}}^2<0$)

A similar set of equations to (16)–(19) can be derived for surface waves. The expansion of the Mathieu functions in terms of Bessel functions for n_{i}^2 (surface waves) are, from McLachlan (1947),

$$\mathrm{Ce}_{2m}(s,m_{\mathrm{i}}^2)=(-1)^m\sum_{r=0}^{\infty}(-1)^rA^{2m}_{2r}(n_{\mathrm{i}}^2)\cosh(2ms), \tag{20}$$

$$\mathrm{Ce}_{2m+1}(s,m_{\mathrm{i}}^2)=(-1)^m\sum_{r=0}^{\infty}(-1)^rB^{2m+1}_{2r+1}(n_{\mathrm{i}}^2)\cosh(2m+1)s, \tag{21}$$

$$\mathrm{Se}_{2m+1}(s,m_{\mathrm{i}}^2)=(-1)^m\sum_{r=0}^{\infty}(-1)^rA^{2m+1}_{2r+1}(n_{\mathrm{i}}^2)\sinh(2m+1)s, \tag{22}$$

$$\mathrm{Se}_{2m+2}(s,m_{\mathrm{i}}^2)=(-1)^m\sum_{r=0}^{\infty}(-1)^rB^{2m+2}_{2r+2}(n_{\mathrm{i}}^2)\sinh(2m+2)s, \tag{23}$$

where $m_{\mathrm{i}}^2=-n_{\mathrm{i}}^2<0$. The coefficients $A^{2m}_{2r}(n_{\mathrm{i}}^2)$, $A^{2m+1}_{2r+1}(n_{\mathrm{i}}^2)$, $B^{2m+2}_{2r+2}(n_{\mathrm{i}}^2)$ and $B^{2m+1}_{2r+1}(n_{\mathrm{i}}^2)$ are related by recurrence relations which can be found in Abramowitz & Stegun (1964). These equations can be substituted in to (16)–(19) to find dispersion relations for surface waves.

3. Thin magnetic tube

In the thin magnetic tube approximation, the length of the tube is much greater than the major axis, i.e. $a=\sigma\cosh(s_0)$, $b=\sigma\sinh(s_0)\ll L$ (or wavelengths are much greater than the major axis). This approximation can be used to simplify the dispersion Eqs. (16)–(19). This means $|m_{\mathrm{i}}^2|\sim|n_{\mathrm{e}}^2|\sim(a/L)^2\ll1$. Now using the expansions for $A_r^q\left(m_{\mathrm{i}}^2\right)$, $B_r^q\left(m_{\mathrm{i}}^2\right)$ for $|m_{\mathrm{i}}^2|,|n_{\mathrm{e}}^2|\ll1$ (Abramowitz & Stegun 1964)

$$A_0^0\left(m_{\mathrm{i}}^2\right)\sim2^{-1/2},\qquad A_r^r\left(m_{\mathrm{i}}^2\right)=B_r^r\left(m_{\mathrm{i}}^2\right)\sim1,$$

$$A_{r+2q}^r\left(m_{\mathrm{i}}^2\right)=B_{r+2q}^r\left(m_{\mathrm{i}}^2\right)\sim O(m_{\mathrm{i}}^n),$$

$$A_{r-2f}^r\left(m_{\mathrm{i}}^2\right)=B_{r-2f}^r\left(m_{\mathrm{i}}^2\right)\sim O(m_{\mathrm{i}}^n), \tag{24}$$

where $r,q=0,1,2,...$ and $f=1,...,[r/2]$ and $[r/2]$ is the integer part of $r/2$.

Substituting the expansions for Fek_0, Fek_n, Gek_n found in Appendix C into (16)–(19) and using (13), (24), (A.3) and (A.4), we obtain the systems of equations

$$2^{1/2}\rho_{\mathrm{i}}(\omega_{\mathrm{Ai}}^2c_i^2-\left(c_i^2+v_{\mathrm{Ai}}^2\right)\omega^2)\alpha_0^i=$$

$$(\ln|n_{\mathrm{e}}|+2s_0+2\gamma-2\ln2)\rho_{\mathrm{e}}\left(\omega_{\mathrm{Ae}}^2c_{\mathrm{e}}^2-\left(c_{\mathrm{e}}^2+v_{\mathrm{Ae}}^2\right)\omega^2\right)E_0,$$

$$\frac{\left(\omega^2-\omega_{\mathrm{e}}^2\right)}{2n_{\mathrm{e}}^2}E_0=0, \tag{25}$$

for $n=0$ representing magneto-acoustic sausage oscillations in a compressible waveguide with an elliptical cross-section, whereas

$$\rho_{\mathrm{i}}\left(\omega_{\mathrm{Ai}}^2c_i^2-\left(c_i^2+v_{\mathrm{Ai}}^2\right)\omega^2\right)\cosh(ns_0)\alpha_n^i=$$

$$\rho_{\mathrm{e}}\left(\omega_{\mathrm{Ae}}^2c_{\mathrm{e}}^2-\left(c_{\mathrm{e}}^2+v_{\mathrm{Ae}}^2\right)\omega^2\right)\mathrm{e}^{-ns_0}E_n,$$

$$\frac{\left(\omega^2-\omega_{\mathrm{i}}^2\right)}{2m_{\mathrm{i}}^2}\sinh(ns_0)\alpha_n^i=-\frac{\left(\omega^2-\omega_{\mathrm{e}}^2\right)}{2n_{\mathrm{e}}^2}\mathrm{e}^{-ns_0}E_n, \tag{26}$$

and

$$\rho_{\mathrm{i}}\left(\omega_{\mathrm{Ai}}^2c_i^2-\left(c_i^2+v_{\mathrm{Ai}}^2\right)\omega^2\right)\sinh(ns_0)\beta_n^i=$$

$$\rho_{\mathrm{e}}\left(\omega_{\mathrm{Ae}}^2c_{\mathrm{e}}^2-\left(c_{\mathrm{e}}^2+v_{\mathrm{Ae}}^2\right)\omega^2\right)\mathrm{e}^{-ns_0}F_n,$$

$$\frac{\left(\omega^2-\omega_{\mathrm{i}}^2\right)}{2m_{\mathrm{i}}^2}\cosh(ns_0)\beta_n^i=\frac{\left(\omega^2-\omega_{\mathrm{e}}^2\right)}{2n_{\mathrm{e}}^2}\mathrm{e}^{-ns_0}F_n, \tag{27}$$

describe magneto-acoustic MHD body waves ($m_{\rm i}^2 > 0$) for the kink mode ($n = 1$) and fluting ($n = 2, 3, 4...$) modes in a compressible waveguide with an elliptical cross-section. The new variables

$$E_0 = \frac{u_0}{\pi}\alpha_0^{\rm e}, \qquad E_{2m-1} = \frac{(-1)^m u_{2m-1}}{\pi|n_{\rm e}|}A_1^{2m-1}\alpha_{2m-1}^{\rm e},$$

$$E_{2m} = \frac{(-1)^m u_{2m}}{2\pi m A_0^{2m}}\alpha_{2m}^{\rm e}$$

$$F_{2m-1} = \frac{(-1)^m q_{2m-1}}{\pi|n_{\rm e}|B_1^{2m-1}}\beta_{2m-1}^{\rm e}, \qquad F_{2m} = \frac{2m(-1)^m q_{2m}}{\pi|n_{\rm e}|B_2^{2m}}\beta_{2m}^{\rm e},$$

have been introduced. Also the variables

$$A_0^{2m}u_{2m} = {\rm ce}_{2m}(0){\rm ce}_{2m+1}(\pi/2),$$

$$|m_{\rm i}|A_1^{2m+1}u_{2m+1} = {\rm ice}_{2m+1}(0){\rm ce}'_{2m+1}(\pi/2),$$

$$|m_{\rm i}|B_1^{2m+1}q_{2m+1} = -{\rm ise}'_{2m+1}(0){\rm se}_{2m+1}(\pi/2),$$

$$m_{\rm i}^2 B_1^{2m+2}q_{2m+2} = {\rm se}'_{2m+2}(0){\rm se}'_{2m+2}(\pi/2),$$

have been introduced.

From an observational point of view, most interest is focused on sausage (i.e. longitudinal, acoustic) and kink (i.e. transverse) modes. Next we will determine how ellipticity may affect the properties (e.g. period, phase speed) of these particular modes.

3.1. Sausage mode (n = 0)

Setting the determinants of each system equal to zero, Eq. (25) gives the dispersion relation for the sausage body modes

$$\frac{2^{1/2}\rho_{\rm i}}{n_{\rm e}^2}\left(\omega^2-\omega_{\rm e}^2\right)\left(\omega^2-\omega_{\rm T}^2\right) = 0. \tag{28}$$

It is clear that there is a mode propagating with phase speed approximately equal to the tube speed $c_{\rm T}$. This mode is the slow body mode which is subsonic but has phase speed greater than the tube speed. Using (20), it can be shown that Eq. (28) also describes the surface waves. Under photospheric conditions (e.g. $v_{\rm Ai} > c_{\rm e} > c_0 \gg v_{\rm Ae}$) a fast surface wave propagating with phase speed $c_{\rm e}$ is allowed as the internal plasma is cooler than the external plasma. Also allowed is a slow surface mode with phase speed equal to $c_{\rm T}$, as $B_{\rm i} \gg B_{\rm e}$. This slow surface mode is subsonic and has phase speed sub tube speed. An explanation of the conditions needed for surface waves to occur can be found in (Roberts 1981).

3.1.1. Slow sausage mode

To investigate how the ellipticity effects the sausage modes, a higher order approximation of the solutions to Eqs. (16) and (17) is required. For the slow body mode with $\omega^2 \approx \omega_{\rm T}^2$, a dispersive correction can be found by using (B.1) and (B.10), then making the approximation for Bessel functions valid for small argument z (Abramowitz & Stegun 1964)

$$J_n(z) \sim \frac{(\frac{1}{2}z)^n}{n!}, \qquad z \ll 1,$$

yielding, after substitution in (16) and (17),

$$2^{1/2}\rho_{\rm i}\left(c_i^2+v_{\rm Ai}^2\right)\left(\omega_{\rm T}^2-\omega^2\right)\alpha_0^i = K_0(|n_{\rm e}|{\rm e}^{s_0})\rho_{\rm e}\left(c_{\rm e}^2+v_{\rm Ae}^2\right)\left(\omega_{\rm Te}^2-\omega^2\right)E_0,$$

$$\sinh(2s_0)\left(\omega^2-\omega_{\rm i}^2\right)\alpha_0^i = -\left(1+n_{\rm e}^2{\rm e}^{-2s_0}K_0(|n_{\rm e}|{\rm e}^{s_0})\right)\times\frac{\left(\omega^2-\omega_{\rm e}^2\right)}{2n_{\rm e}^2}E_0.$$

The dispersive correction for $\omega^2 \approx \omega_{\rm T}^2$ can then be written as

$$\omega^2 = \omega_{\rm T}^2\left\{1+\frac{k^2a^3b}{4(a^2+b^2)}\frac{\rho_{\rm e}}{\rho_{\rm i}} \times K_0\left(|n_{\rm e}|{\rm e}^{(2/\epsilon-2)^{1/2}}\right)\frac{(c_{\rm T}^2-c_{\rm i}^2)\left(c_{\rm T}^2-v_{\rm Ae}^2\right)}{\left(c_{\rm i}^2+v_{\rm Ai}^2\right)c_{\rm T}^2}\right\}, \tag{29}$$

where $s_0 \approx (2/\epsilon-2)^{1/2}$ valid for small s_0 and from Eq. (4) it can be found that $\sigma^2 \sim a^4/(a^2+b^2)$. The phase speed of the slow body sausage mode is shown for various values of ellipticity in Figs. 3–5. The dispersive correction for the slow surface sausage mode, also with $\omega^2 \approx \omega_{\rm T}^2$, is given by

$$\omega^2 = \omega_{\rm T}^2\left\{1-\frac{k^2a^3b}{4(a^2+b^2)}\frac{\rho_{\rm e}}{\rho_{\rm i}} \times K_0\left(|n_{\rm e}|{\rm e}^{(2/\epsilon-2)^{1/2}}\right)\frac{(c_{\rm T}^2-c_{\rm i}^2)\left(v_{\rm Ae}^2-c_{\rm T}^2\right)}{\left(c_{\rm i}^2+v_{\rm Ai}^2\right)c_{\rm T}^2}\right\}. \tag{30}$$

For both the body (29) and surface (30) waves the ellipticity has a small but clear effect. Increasing ellipticity increases (decreases) the frequencies and phase speeds of the slow body (surface) waves.

3.1.2. Fast sausage mode

Consider the fast surface sausage mode with phase speed close to $c_{\rm e}$. An expression can be developed from Eqs. (16) and (17), using the approximation of the Mathieu functions with Bessel functions found in Appendix B, for the ellipticity correction of the mode with $\omega^2 \approx \omega_{\rm e}^2$:

$$\omega^2 = \omega_{\rm e}^2\left\{1-k^2\frac{\rho_{\rm e}}{\rho_{\rm i}}{\rm e}^{2(2/\epsilon-2)^{1/2}}\frac{\left(c_{\rm e}^2-c_{\rm i}^2\right)c_{\rm e}^2}{\left(c_{\rm i}^2+v_{\rm Ai}^2\right)\left(c_{\rm e}^2-c_{\rm T}^2\right)}\right\}. \tag{31}$$

It is clear from (31) that there is no dependence on wavenumber k for the frequency and phase speed of this mode. Figures 3a and 4 reflect this for phase speed in the limit $ka \ll 1$.

By considering Eq. (28) and Fig. 3b, it is clear that in the thin tube approximation ($ka \ll 1$) there is no fast sausage mode for coronal conditions. However, the fast sausage mode does exist for large wavenumbers that are greater than a propagation cutoff value. The wavenumber of the propagation cutoffs are given by

$$k = k_{\rm c} \equiv \left[\frac{\left(c_{\rm i}^2+v_{\rm Ai}^2\right)\left(v_{\rm Ae}^2-c_{\rm T}^2\right)}{\left(v_{\rm Ae}^2-c_{\rm i}^2\right)\left(v_{\rm Ae}^2-v_{\rm Ai}^2\right)}\right]^{1/2}\frac{2}{\sigma}{\rm e}^{-(2/\epsilon-2)^{1/2}}j_{0,s}, \tag{32}$$

where $s = 1, 2, 3, ...$ and $j_{0,s} = (2.40, 5.52, ...)$ are the zeros of the Bessel function J_0 found in the function ${\rm Ce}_n\left(s_0, m_{\rm i}^2\right)$ (see Eq. (B.1), the expansion in terms of Bessel functions). It can be seen from Eq. (32) that the cutoff value increases with increasing

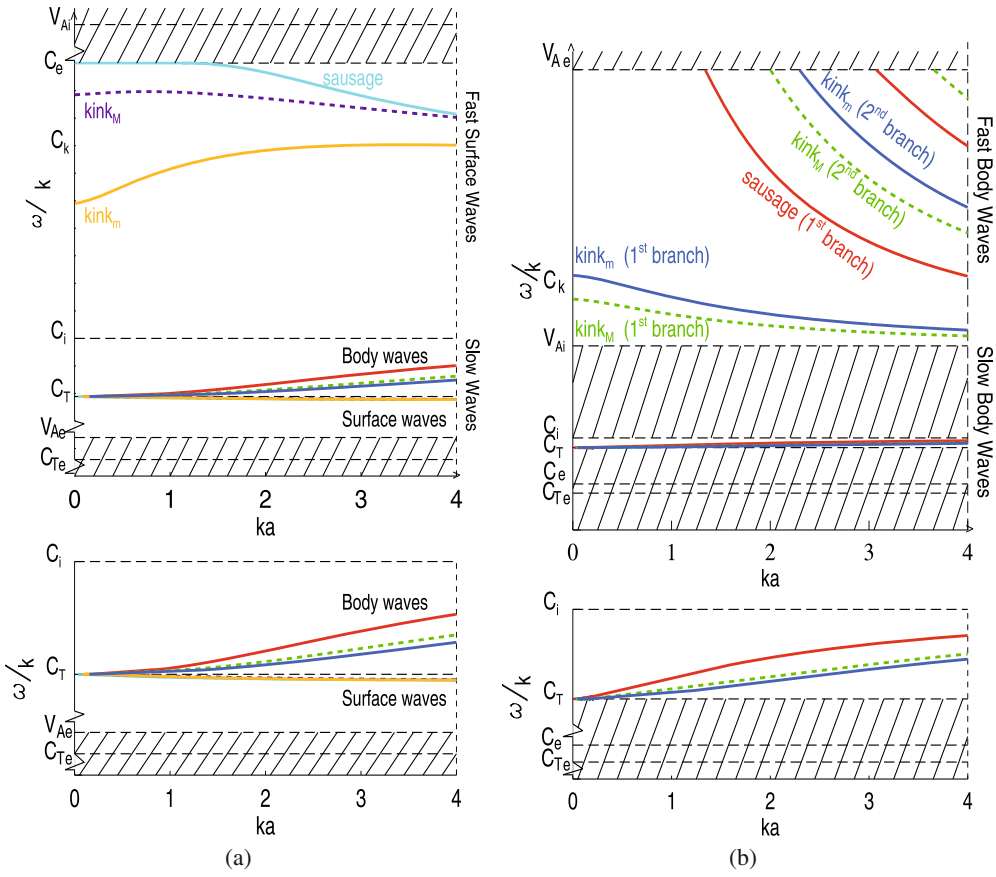

Fig. 3. a) The *left column* shows the phase speeds of modes under photospheric conditions (i.e. $v_{\rm Ai} > c_{\rm e} > c_{\rm i} > v_{\rm Ae}$) for $\epsilon = 0.65$ ($s_0 = 1.0$). The *bottom left panel* shows a magnification of the section showing the slow body and surface waves. The various speeds where taken to be $v_{\rm Ai} = 2c_{\rm i}$, $c_{\rm e} = 1.5c_{\rm i}$ and $v_{\rm Ae} = 0.5c_{\rm i}$ with $B_{\rm i} = 9B_{\rm e}$. Hatching denotes regions where free modes are excluded. **b)** The *right column* shows the phase speeds of modes under coronal conditions (i.e. $v_{\rm Ae} > v_{\rm Ai} > c_{\rm i} > c_{\rm e}$) with $\epsilon = 0.65$ ($s_0 = 1.0$) are shown. The *bottom right panel* shows a magnification of the section showing the slow body waves. The various speeds where taken to be $v_{\rm Ae} = 5c_{\rm i}$, $c_{\rm e} = 0.5c_{\rm i}$ and $v_{\rm Ai} = 2c_{\rm i}$ and $B_{\rm i} = B_{\rm e}$. Both dispersion diagrams are calculated under the assumptions $m_{\rm i}$ and $m_{\rm e}$ are small.

ellipticity. As the ellipticity tends to zero, we obtain the cutoff value found for the circular cross-section (Roberts et al. 1984). For large ellipticity (small s_0) we obtain the approximation

$$k = k_{\rm c} \equiv k_{c({\rm cylinder})} + \left[\frac{\left(c_{\rm i}^2 + v_{\rm Ai}^2\right)\left(v_{\rm Ae}^2 - c_{\rm T}^2\right)}{\left(v_{\rm Ae}^2 - c_{\rm i}^2\right)\left(v_{\rm Ae}^2 - v_{\rm Ai}^2\right)}\right]^{1/2} \times \frac{j_{0,s}}{a}\left(1 - 2(2/\epsilon - 2)^{1/2}\right), \quad (33)$$

which is written in terms of the cylindrical cutoff plus the leading order term from the ellipticity.

Consider now the focal points of the elliptical cross-section. It is known that sausage oscillations do not perturb the axis of the cylindrical magnetic flux tube. In elliptical geometry there is, of course, no rotational symmetry for perturbations. Instead, the magnetic field lines passing through the focal points may be considered as the elliptical counterparts of the field lines representing the axis of the cylinder in a flux tube with a circular cross-section. The x and y components of velocity are obtained, for the sausage mode ($n = 0$):

$$\hat{v}_x(s,\varphi) = 0, \qquad \hat{v}_y(s,\varphi) = 0;$$

and the higher modes ($n > 0$):

$$\hat{v}_x(0,0) = n\left(A_n^n\left(m_{\rm i}^2\right)\right)^2 \frac{\left(\omega_{\rm i}^2 - \omega^2\right)}{\sigma\omega^2 m_{\rm i}^2}, \qquad \hat{v}_y(0,0) = 0,$$

$$\hat{v}_x(0,\pi) = n\left(A_n^n\left(m_{\rm i}^2\right)\right)^2 \frac{\left(\omega_{\rm i}^2 - \omega^2\right)}{2\sigma\omega^2 m_{\rm i}^2}(1 - \cos n\pi), \quad (34)$$

$$\hat{v}_y(0,\pi) = n\left(B_n^n\left(m_{\rm i}^2\right)\right)^2 \frac{\left(\omega_{\rm i}^2 - \omega^2\right)}{2\sigma\omega^2 m_{\rm i}^2}(1 + \cos n\pi),$$

for the perturbations associated with $\hat{\Delta} = {\rm Ce}_n(s, m_{\rm i}^2){\rm ce}_n\left(\varphi, m_{\rm i}^2\right)$ and

$$\hat{v}_x(0,0) = 0, \qquad \hat{v}_y(0,0) = n\left(B_n^n\left(m_{\rm i}^2\right)\right)^2 \frac{\left(\omega_{\rm i}^2 - \omega^2\right)}{\sigma\omega^2 m_{\rm i}^2},$$

$$\hat{v}_x(0,\pi) = -n\left(B_n^n\left(m_{\rm i}^2\right)\right)^2 \frac{\left(\omega_{\rm i}^2 - \omega^2\right)}{2\sigma\omega^2 m_{\rm i}^2}(1 + \cos n\pi), \quad (35)$$

$$\hat{v}_y(0,\pi) = n\left(B_n^n\left(m_{\rm i}^2\right)\right)^2 \frac{\left(\omega_{\rm i}^2 - \omega^2\right)}{2\sigma\omega^2 m_{\rm i}^2}(1 - \cos n\pi).$$

for the perturbations associated with $\hat{\Delta} = Se_n(s, m_{\rm i}^2)se_n\left(\varphi, m_{\rm i}^2\right)$. So, for the higher modes there is movement of the focal points in both the s and φ directions. One could generalise the definition of the sausage mode: wave propagation or oscillation that does not perturb the focal points; and the higher (fluting) modes: wave

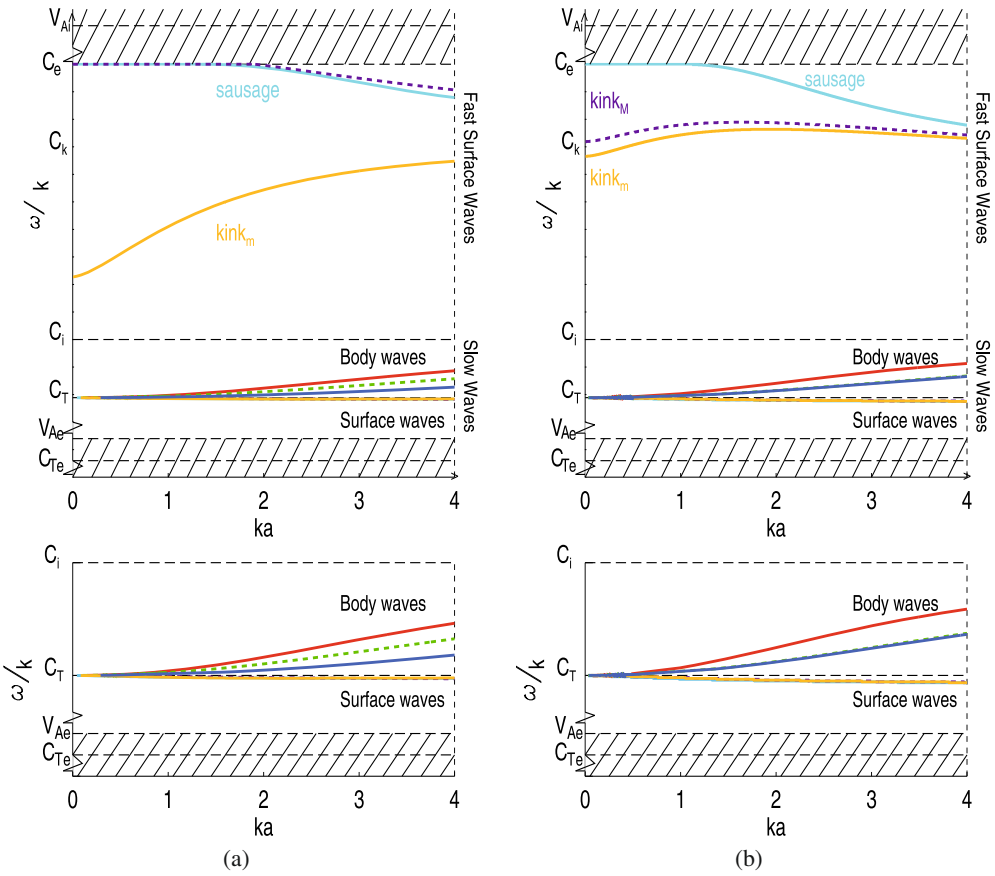

Fig. 4. The phase speeds of modes under photospheric conditions for **a)** $\epsilon = 0.84$ ($s_0 = 0.6$) and **b)** $\epsilon = 0.27$ ($s_0 = 2.0$). Both dispersion diagrams are calculated under the assumptions m_i and m_e are small.

propagation or oscillation that perturbs the focal points. For $n = 1$ (kink) in particular, Eqs. (34) show perturbations polarised in the x-directions and Eqs. (35) show perturbations polarised in the y-direction.

3.2. Kink mode

Setting the determinants of Eqs. (26) and (27) equal to zero, two equations can be obtained that describe the kink body modes,

$$\rho_e \frac{\tanh(s_0)}{\left(\omega^2 - \omega_{Ai}^2\right)} - \rho_i \frac{1}{\left(\omega^2 - \omega_{Ae}^2\right)} = 0, \tag{36}$$

and

$$\rho_e \frac{\coth(s_0)}{\left(\omega^2 - \omega_{Ai}^2\right)} - \rho_i \frac{1}{\left(\omega^2 - \omega_{Ae}^2\right)} = 0. \tag{37}$$

Ruderman (2003) found these expressions for a cold plasma and determined that (36) describes the kink mode polarised along the major axis, while (37) describes the kink mode polarised along the minor axis. By considering Eqs. (21) and (22), the equations that describe the kink surface waves can also be found. From now on, the kink modes linearly polarised in the direction of the major axis will be labeled ω_{1M} and the kink modes linearly polarised in the direction of the minor axis ω_{1m}. However, it is not immediately obvious what the solutions to Eqs. (36) and (37) are. Keeping in mind the kink modes found for cylindrical case (Edwin & Roberts 1983), we investigate the nature of the kink modes present in a flux tube with elliptical cross-section.

3.2.1. Slow kink mode

Under the supposition there is a solution $\omega \approx \omega_T$, consider two sets of dispersion relations (16)–(19) for $n = 1$. There is the possibility that m_i^2 remains finite as $\pi a/L \to 0$. Substituting Eqs. (B.2) and (B.3), (B.11) and (B.12) into (16)–(19), we obtain

$$m_i X_{1,2} = -\frac{\rho_i}{\rho_e} \frac{\left(\omega_T^2 - \omega_{Ai}^2\right)}{\left(\omega_T^2 - \omega_{Ae}^2\right)}, \tag{38}$$

where

$$m_i X_1 = \frac{\mathrm{Ce}_1'}{\mathrm{Ce}_1}, \qquad m_i X_2 = \frac{\mathrm{Se}_1'}{\mathrm{Se}_1}.$$

After squaring and rearranging, Eq. (38) can be recast as

$$\omega_{1M}^2 = \omega_T^2 \left\{ 1 + \frac{a^4 k^2 \rho_e^2}{4\rho_i^2 (a^2 + b^2)} \frac{\left(c_T^2 - v_{Ae}^2\right)^2 \left(c_T^2 - c_i^2\right) X_1^2}{\left(c_i^2 + v_{Ai}^2\right)\left(c_T^2 - v_{Ai}^2\right) c_T^2} \right\}, \tag{39}$$

$$\omega_{1m}^2 = \omega_T^2 \left\{ 1 + \frac{a^4 k^2 \rho_e^2}{4\rho_i^2 (a^2 + b^2)} \frac{\left(c_T^2 - v_{Ae}^2\right)^2 \left(c_T^2 - c_i^2\right) X_2^2}{\left(c_i^2 + v_{Ai}^2\right)\left(c_T^2 - v_{Ai}^2\right) c_T^2} \right\}. \tag{40}$$

These equations determine the slow kink body modes for photospheric and coronal conditions. It can be seen from Eqs. (39) and (40) that the slow kink modes are weakly dependent on ellipticity and both equations tend to c_T as $ka \to 0$, regardless of the value of ellipticity (see the bottom panels in Figs. 3–5). This is

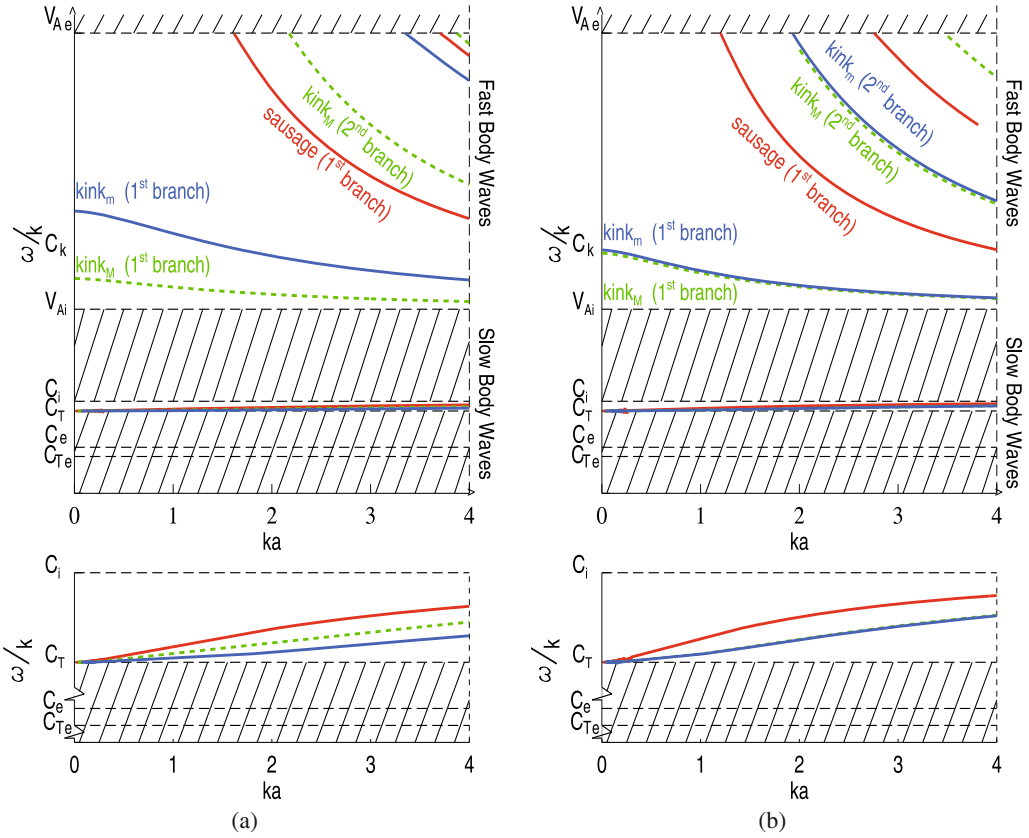

Fig. 5. The phase speeds of modes under coronal conditions for **a)** $\epsilon = 0.89$ ($s_0 = 0.5$) and **b)** $\epsilon = 0.27$ ($s_0 = 2.0$). Both dispersion diagrams are calculated under the assumptions m_i and m_e are small.

because the slow magneto-acoustic waves are polarised mainly longitudinally, along the field lines, and are less affected by the change in shape of the cross-section in the first order approximation. For the slow kink surface wave the ellipticity correction is given by:

$$\omega_{1M}^2 = \omega_T^2 \left\{ 1 - \frac{a^4 k^2 \rho_e^2}{4\rho_i^2 (a^2+b^2)} \frac{\left(c_T^2 - v_{Ae}^2\right)^2 \left(c_T^2 - c_i^2\right) X_1^2}{\left(c_i^2 + v_{Ai}^2\right)\left(c_T^2 - v_{Ai}^2\right) c_T^2} \right\}, \tag{41}$$

$$\omega_{1m}^2 = \omega_T^2 \left\{ 1 - \frac{a^4 k^2 \rho_e^2}{4\rho_i^2 (a^2+b^2)} \frac{\left(c_T^2 - v_{Ae}^2\right)^2 \left(c_T^2 - c_i^2\right) X_2^2}{\left(c_i^2 + v_{Ai}^2\right)\left(c_T^2 - v_{Ai}^2\right) c_T^2} \right\}, \tag{42}$$

In the limit $a/b \to 1$ corresponding to the circular-cross section we obtain from Eqs. (39) and (40)

$$\omega_{1M}^2 = \omega_{1m}^2 = \omega_T^2 \left\{ 1 + \frac{a^2 k^2 \rho_e^2}{2\rho_i^2} \frac{\left(c_T^2 - v_{Ae}^2\right)^2 \left(c_T^2 - c_i^2\right) X_1^2}{\left(c_i^2 + v_{Ai}^2\right)\left(c_T^2 - v_{Ai}^2\right) c_T^2} \right\},$$

where $X_1^2 \approx X_2^2$. Again, in this limit the result for the slow kink mode in a cylinder (Edwin & Roberts 1983) is recovered, with $X_1^2 \approx m_i(I_0(m_i a)/I_1(m_i a) - 1)$.

3.2.2. Fast kink mode

Observationally the fast kink mode is perhaps the best studied, since their spectacular discoveries by TRACE. Consider now the possiblilty $m_i^2 a \to 0$ as $ka \to 0$. The Eqs. (36) and (37) then determine the dispersion relation for the fast kink modes and reduce to

$$\omega^2 = \omega_{1M}^2 = \frac{b\rho_e \omega_{Ae}^2 + a\rho_i \omega_{Ai}^2}{a\rho_i + b\rho_e} \tag{43}$$

$$\omega^2 = \omega_{1m}^2 = \frac{b\rho_i \omega_{Ai}^2 + a\rho_e \omega_{Ae}^2}{a\rho_e + b\rho_i} \tag{44}$$

where a and b are the large and small half axis, respectively, of the elliptic cross-section. These equations describe the fast body waves for coronal conditions ($v_{Ae}, v_{Ai} \gg c_i, c_e$). Eq. (43) describes the kink mode polarised along the x-axis (major), while Eq. (44) describes the kink mode polarised along the y-axis (minor). These solutions are the same in leading order as the dispersion relations for the kink modes in a cold plasma (Ruderman 2003), which is expected as the kink modes are highly incompressible in linear MHD.

The different phase speeds for the kink modes perturbing the two axis can be seen clearly in Fig. 3. The difference in phase speeds increases as the ellipticity increases (compare Fig. 5b for $\epsilon = 0.89$ to Fig. 3b with $\epsilon = 0.65$). Taking the limits of Eqs. (43) and (44) when the ellipticity tends to one (i.e. $b/a \to 0$), we find

$$\omega_{1M} = \omega_{Ai}, \qquad \omega_{1m} = \omega_{Ae}.$$

This result also corresponds well to the counterpart found for the kink mode for the magnetic slab (Edwin & Roberts 1982). For discussion on the physical reason for this see Ruderman (2003). For small values of ellipticity, the phase speeds for the two axis tend to the same value (compare Fig. 5b for $\epsilon = 0.27$ to Fig. 3b).

If we let $\epsilon \to 0$, $(a/b \to 1)$ which corresponds to a flux tube with a circular cross-section. In this limit Eqs. (43), (44) both tend to

$$\omega_{1\mathrm{M}}^2 = \omega_{1\mathrm{m}}^2 = \frac{\rho_\mathrm{i}\omega_\mathrm{Ai}^2 + \rho_\mathrm{e}\omega_\mathrm{Ae}^2}{\rho_\mathrm{e} + \rho_\mathrm{i}}$$

which is the frequency of kink oscillations in a thin tube with a circular cross-section (Spruit 1982; Edwin & Roberts 1983).

The Eqs. (43) and (44) also describe the fast surface waves under photospheric conditions (can be seen by considering Eqs. (B.4) and (B.5)). The phase speeds for a photospheric case are shown for various values of ellipticity in Figs. 3a and 4. The difference in phase speeds for the kink mode along the two axis is also present for surface waves in the photosphere and responds in a similar manner to an increase/decrease in ellipticity. However, $c_{\mathrm{kM}} > c_{\mathrm{km}}$ for the surface waves whereas for for body waves in the corona $c_{\mathrm{km}} > c_{\mathrm{kM}}$. This is due to the relative strengths of the internal and external magnetic fields in the corona and photosphere.

Equations (43) and (44) however do not show how the fast kink modes vary with wavenumber. To investigate the relationship we need to find a higher order equation. Consider now the mode with phase speed $c \approx c_\mathrm{k}$. A dispersive correction for the body waves of this mode can be found by writing Eqs. (16) and (17) as

$$\omega_{1\mathrm{M}}^2 = k^2\left(v_\mathrm{Ae}^2 - \frac{\rho_\mathrm{i}}{\rho_\mathrm{e}}v_\mathrm{Ai}^2\Psi_1\right)\left(1 + \frac{\rho_\mathrm{i}}{\rho_\mathrm{e}}\Psi_1\right)^{-1},$$

and (18), (19) as

$$\omega_{1\mathrm{m}}^2 = k^2\left(v_\mathrm{Ae}^2 - \frac{\rho_\mathrm{i}}{\rho_\mathrm{e}}v_\mathrm{Ai}^2\tilde{\Psi}_1\right)\left(1 + \frac{\rho_\mathrm{i}}{\rho_\mathrm{e}}\tilde{\Psi}_1\right)^{-1},$$

where

$$\begin{aligned}\Psi_1 &= \frac{\mathrm{Ce}_1\left(s_0, m_\mathrm{i}^2\right)\mathrm{Fek}_1'\left(s_0, n_\mathrm{e}^2\right)}{\mathrm{Ce}_1'\left(s_0, m_\mathrm{i}^2\right)\mathrm{Fek}_1\left(s_0, n_\mathrm{e}^2\right)}\\ &= \coth(s_0)\left\{K_0(|n_\mathrm{e}|\mathrm{e}^{s_0})\left(1 - \frac{\mathrm{e}^{-2s_0}}{2}\right)\frac{n_\mathrm{e}^2\mathrm{e}^{2s_0}}{2} + 1\right\},\end{aligned}$$

and

$$\begin{aligned}\tilde{\Psi}_1 &= \frac{\mathrm{Se}_1\left(s_0, m_\mathrm{i}^2\right)\mathrm{Gek}_1'\left(s_0, n_\mathrm{e}^2\right)}{\mathrm{Se}_1'\left(s_0, m_\mathrm{i}^2\right)\mathrm{Gek}_1\left(s_0, n_\mathrm{e}^2\right)}\\ &= \tanh(s_0)\left\{K_0(|n_\mathrm{e}|\mathrm{e}^{s_0})\left(1 + \frac{\mathrm{e}^{-2s_0}}{2}\right)\frac{n_\mathrm{e}^2\mathrm{e}^{2s_0}}{2} + 1\right\}.\end{aligned}$$

Here we have used the expansions (B.2), (B.3), (B.8) and (B.9). The dispersive corrections are then given by

$$\begin{aligned}\omega_{1\mathrm{M}}^2 = k^2c_{\mathrm{kM}}^2\Bigg\{1 - \frac{\rho_\mathrm{e}\rho_\mathrm{i}}{2}\frac{\left(bv_\mathrm{Ae}^2 - av_\mathrm{Ai}^2\right)}{\left(b\rho_\mathrm{e} + a\rho_\mathrm{i}\right)^2c_{\mathrm{kM}}^2}\\ \times K_0\left(\sigma\lambda\frac{k}{2}\mathrm{e}^{(2/\epsilon-2)^{1/2}}\right)\left(\mathrm{e}^{2(2/\epsilon-2)^{1/2}} - \frac{1}{2}\right)\frac{(\sigma\lambda k)^2}{4}\Bigg\},\end{aligned} \tag{45}$$

and

$$\begin{aligned}\omega_{1\mathrm{m}}^2 = k^2c_{\mathrm{km}}^2\Bigg\{1 - \frac{\rho_\mathrm{e}\rho_\mathrm{i}}{2}\frac{\left(av_\mathrm{Ae}^2 - bv_\mathrm{Ai}^2\right)}{\left(a\rho_\mathrm{e} + b\rho_\mathrm{i}\right)^2c_{\mathrm{km}}^2}\\ \times K_0\left(\sigma\lambda\frac{k}{2}\mathrm{e}^{(2/\epsilon-2)^{1/2}}\right)\left(\mathrm{e}^{2(2/\epsilon-2)^{1/2}} - \frac{1}{2}\right)\frac{(\sigma\lambda k)^2}{4}\Bigg\}.\end{aligned} \tag{46}$$

Here

$$c_{\mathrm{kM}}^2 = \frac{\left(b\rho_\mathrm{e}v_\mathrm{Ae}^2 + av_\mathrm{Ai}^2\rho_\mathrm{i}\right)}{b\rho_\mathrm{e} + a\rho_\mathrm{i}}, \qquad c_{\mathrm{km}}^2 = \frac{\left(a\rho_\mathrm{e}v_\mathrm{Ae}^2 + bv_\mathrm{Ai}^2\rho_\mathrm{i}\right)}{a\rho_\mathrm{e} + b\rho_\mathrm{i}},$$

are the kink speeds modified by ellipticity. Also

$$\lambda^2 = \frac{\left(c_\mathrm{k}^2 - c_\mathrm{e}^2\right)\left(c_\mathrm{k}^2 - v_\mathrm{Ae}^2\right)}{\left(c_\mathrm{e}^2 + v_\mathrm{Ae}^2\right)\left(c_\mathrm{k}^2 - c_\mathrm{Te}^2\right)}.$$

Equations (45) and (46) show the relationship between frequency (hence phase speed) and $ka = \pi/L$, and shows that the frequency decreases as ka increases. The dispersive correction for surface waves can be found by following a similar procedure.

Taking the limit $s_0 \to \infty$, using $\exp(s_0) = (a + b)/\sigma$ we see

$$\omega_{1\mathrm{M}}^2 = \omega_{1\mathrm{m}}^2 = k^2c_\mathrm{k}^2\left\{1 - \frac{\rho_\mathrm{e}\rho_\mathrm{i}}{2}\frac{\left(v_\mathrm{Ae}^2 - v_\mathrm{Ai}^2\right)}{(\rho_\mathrm{e} + \rho_\mathrm{i})^2c_\mathrm{k}^2}K_0(\lambda ka)(\lambda ak)^2\right\},$$

which is the dispersive correction obtained for a magnetic cylinder (Edwin & Roberts 1983).

3.2.3. Frequency ratio

With present observational technology, identification of fast kink oscillations in the solar atmosphere provides the least problems compared to the fast sausage or slow modes. One would also expect the identification of a flux tube with an elliptical cross-section to be more likely from the fast kink oscillations due to there being two separately polarised oscillations. On comparison between $\omega_{1\mathrm{M}}$ and $\omega_{1\mathrm{m}}$ the ratio is given by

$$\begin{aligned}\frac{\omega_{1M,j}}{\omega_{1m,j}} = \left(\frac{b}{a} + \frac{\rho_\mathrm{e}}{\rho_\mathrm{i}}\right)^{1/2}\Bigg\{1 + \frac{(b\rho_\mathrm{e}j\sigma\lambda k)^2}{16a^2\rho_\mathrm{i}}\\ \times\frac{K_0\left(\sigma\lambda\frac{jk}{2}\mathrm{e}^{(2/\epsilon-2)^{1/2}}\right)\left(\mathrm{e}^{2(2/\epsilon-2)^{1/2}} - \frac{1}{2}\right)}{\left(1 + \frac{b}{a}\right)\left(\rho_\mathrm{e} + \frac{b}{a}\rho_\mathrm{i}\right)}\Bigg\}\end{aligned} \tag{47}$$

where

$$\begin{aligned}\omega_{1M,j}^2 = (jk)^2c_{\mathrm{kM}}^2\Bigg\{1 - \frac{\rho_\mathrm{e}\rho_\mathrm{i}}{2}\frac{\left(bv_\mathrm{Ae}^2 - av_\mathrm{Ai}^2\right)}{\left(b\rho_\mathrm{e} + a\rho_\mathrm{i}\right)^2c_{\mathrm{kM}}^2}\\ \times K_0\left(\sigma\lambda\frac{jk}{2}\mathrm{e}^{(2/\epsilon-2)^{1/2}}\right)\left(\mathrm{e}^{2(2/\epsilon-2)^{1/2}} - \frac{1}{2}\right)\frac{(j\sigma\lambda k)^2}{4}\Bigg\},\end{aligned} \tag{48}$$

and

$$\begin{aligned}\omega_{1m,j}^2 = (jk)^2c_{\mathrm{km}}^2\Bigg\{1 - \frac{\rho_\mathrm{e}\rho_\mathrm{i}}{2}\frac{\left(av_\mathrm{Ae}^2 - bv_\mathrm{Ai}^2\right)}{\left(a\rho_\mathrm{e} + b\rho_\mathrm{i}\right)^2c_{\mathrm{km}}^2}\\ \times K_0\left(\sigma\lambda\frac{jk}{2}\mathrm{e}^{(2/\epsilon-2)^{1/2}}\right)\left(\mathrm{e}^{2(2/\epsilon-2)^{1/2}} - \frac{1}{2}\right)\frac{(j\sigma\lambda k)^2}{4}\Bigg\}\end{aligned} \tag{49}$$

are the frequencies for the higher harmonics of the fast kink waves. Here $j = 1, 2, 3...$ corresponds to the mode number. For typical coronal conditions and length scales i.e. $L = 100$ Mm, $a = 1$ Mm, and with $\epsilon = 0.87$, the ratio for the fundamental mode $\omega_{1\mathrm{M},1}/\omega_{1\mathrm{m},1} \approx 0.71$. Observations of fast kink modes find the period of loops to be around 276 s (Aschwanden et al. 1999). Assuming this period is due to horizontal motion corresponding $\omega_{1\mathrm{m},1}$, it would be expected that there is a period of 389 s corresponding to $\omega_{1\mathrm{M},1}$ in the vertical direction. If this period is due

to horizontal motion corresponding $\omega_{1M,1}$, then a period of 196 s corresponding to $\omega_{1m,1}$ is expected in the vertical direction. This difference in period is detectable (in principle) with the current cadences available on the TRACE satellite, so the detection of two distinct frequencies, would indicate the possibility of an elliptical cross-section.

Multi-mode oscillations interpreted as harmonics of standing kink modes have been detected in coronal loops (e.g. Verwichte et al. 2004), where two loops were seen to oscillate in the fundamental and first harmonic. For uniform loops, the ratio of the period of the fundamental to the period of the first harmonic is 2. However, the ratios found, by e.g.Verwichte et al. (2004), are 1.64 and 1.81. This may be caused by the geometrical and/or physical effects briefly outlined in the Introduction. Let us now briefly investigate how ellipticity would influence the frequency ratio. The ratio of the first harmonic ($j = 2$) to the fundamental mode ($j = 1$) for the lowest order correction is given by

$$\frac{\omega_{1M,2}}{\omega_{1M,1}} \approx 2(1-\alpha\epsilon^2),$$

$$\alpha = \frac{3a^2\lambda^2k^2}{16}\frac{\rho_e\rho_i}{2}\frac{\left(bv_{Ae}^2 - av_{Ai}^2\right)}{(b\rho_e + a\rho_i)^2\, c_{kM}^2} \times K_0\left(\sigma\lambda\frac{k}{2}e^{(2/\epsilon-2)^{1/2}}\right)\left(e^{2(2/\epsilon-2)^{1/2}} - \frac{1}{2}\right), \quad (50)$$

for the kink major and

$$\frac{\omega_{1m,2}}{\omega_{1m,1}} \approx 2(1-\beta\epsilon^2),$$

$$\beta = \frac{3a^2\lambda^2k^2}{16}\frac{\rho_e\rho_i}{2}\frac{\left(av_{Ae}^2 - bv_{Ai}^2\right)}{(a\rho_e + b\rho_i)^2\, c_{km}^2} \times K_0\left(\sigma\lambda\frac{k}{2}e^{2(2/\epsilon-2)^{1/2}}\right)\left(e^{(2/\epsilon-2)^{1/2}} - \frac{1}{2}\right), \quad (51)$$

for the kink minor. For typical coronal conditions and length scales i.e. $L = 100$ Mm, $a = 1$ Mm, and $\epsilon = 0.87$, then it is found $\alpha, \beta < 0$ and clearly $\omega_2/\omega_1 > 2$. To the best of our knowledge there is no observational data with a claim that $\omega_2/\omega_1 > 2$.

4. Elliptical vs. circular

It is possible to gain insight into the structure present within a magnetic flux tube by measuring the period (or frequency) of oscillations taking place in the tube. This methodology is called magneto-seismology and applying it to coronal loops is called coronal seismology. Inverting the measured periods may provide us with information about the structure of the loop because certain features (i.e. cross-section, curvature, stratification, expansion, varying background, wave leakage, etc.) will cause the period to differ from that of the period calculated for an ideal magnetic cylinder (Edwin & Roberts 1983).

On comparison between the elliptical and the circular cross-section for different values of ka, the phase speeds are found to differ for all modes. So it is expected that there is a difference between the periods of e.g. the well established standing oscillations of the circular cross-sections and elliptical cross-section. The period of the fundamental mode is given by

$$P = \frac{2L}{C_p} \quad (52)$$

where L is the loop length and C_p is the phase speed of a given mode. The percentage difference between the periods for different values of ellipticity are plotted in Fig. 6a for photospheric conditions (i.e. $v_{Ai} > c_e > c_i > v_{Ae}$ with $v_{Ai} = 2c_i$, $c_e = 1.5c_i$ and $v_{Ae} = 0.5c_i$ and $B_i > B_e$) and in Fig. 6b for coronal conditions (i.e. $v_{Ae} > v_{Ai} > c_i > c_e$ with $v_{Ae} = 5c_i$, $c_e = 0.5c_i$ and $v_{Ai} = 2c_i$ and $B_i = B_e$). The periods for the elliptical cross section are calculated under the assumptions m_i and m_e are small. It is expected that these values will not change significantly if calculated without this assumption. The velocity relations that characterise the cylinder were the same used by Edwin & Roberts (1983). The figures show only the fast modes. This is because the difference in phase speeds between the slow modes is too small and it is unlikely that the small difference in phase speeds could be detected with current time resolution and cadence of observational instruments. The percentage difference was calculated using $P_\delta = P_\epsilon/P_c - 1$ where P_δ is the difference in period, P_ϵ is the elliptical period, P_c is the period of the cylinder. In Fig. 6a, the difference in period for the kink major $\epsilon = 0.27$ starts at around $ka = 1.9$. This occurs as the kink major mode has a propagation cutoff as the ellipticity increases (see Fig. 4a).

For increasing ellipticity, one can see that there is an increase in the difference between periods for all modes. In the corona the difference between the periods of the sausage and both kink mode becomes smaller as ka increases. The same happens for the kink modes in the photosphere. This is due to shorter wavelengths feeling the effect of the geometry of the cross-section less then longer wavelengths. For the sausage mode in the photosphere, the period is seen to increase as ka increases. However, it is expected that the difference in period decreases for greater ka than shown. By considering the sausage mode in Fig. 4a, the phase speed seems to tend to the same limit as the phase speed of the kink modes as ka increases. From Fig. 6a, the difference in period of the kink modes tends to zero as ka increases, i.e. it tends to the period of the kink mode of the cylinder. The sausage mode of a flux tube with elliptical cross-section then must also tend to this limit and hence will be the same as the sausage mode for the cylinder. It follows that the difference in period will then tend to zero at greater ka.

As an example, consider a typical loop of length $L = 100$ Mm under coronal conditions with $B = 20$ G, electron density $n_e = 1 \times 10^9$ cm^{-3}. The period for the fast kink mode of the cylinder is given by Roberts et al. (1984),

$$P = \frac{2L}{c_k} = C_f\left(\frac{LN_0^{1/2}}{B_i}\right),$$

where $C_f = 6.5 \times 10^{-12}$ cgs units and we assume $\rho_i \gg \rho_e$ and $B_i \approx B_e$. Using typical characteristic coronal values, we find $P = 103$ s. However, if the loop had an elliptical cross-section with $\epsilon = 0.89$ corresponding to major axis a twice the length of minor axis b, one would expect to see periods of $P = 125$ s from the major axis and $P = 91$ s from the minor axis.

5. Concluding remarks

In this paper the vibrational modes of an elliptical magnetic flux tubes embedded in a magnetic environment with a finite plasma beta is discussed. It was found that a flux tube with elliptical cross-section has an even richer variety of magneto-acoustic modes than those found in the magnetic cylinder.

The flux tube with an elliptical cross-section supports the slow and fast body sausage mode and the slow and fast surface sausage modes, which where not seen in the thin tube approximation of the cold plasma case (Ruderman 2003). The phase speed of all the sausage modes was found to vary with ellipticity. Dispersive corrections for the slow waves and fast surface wave

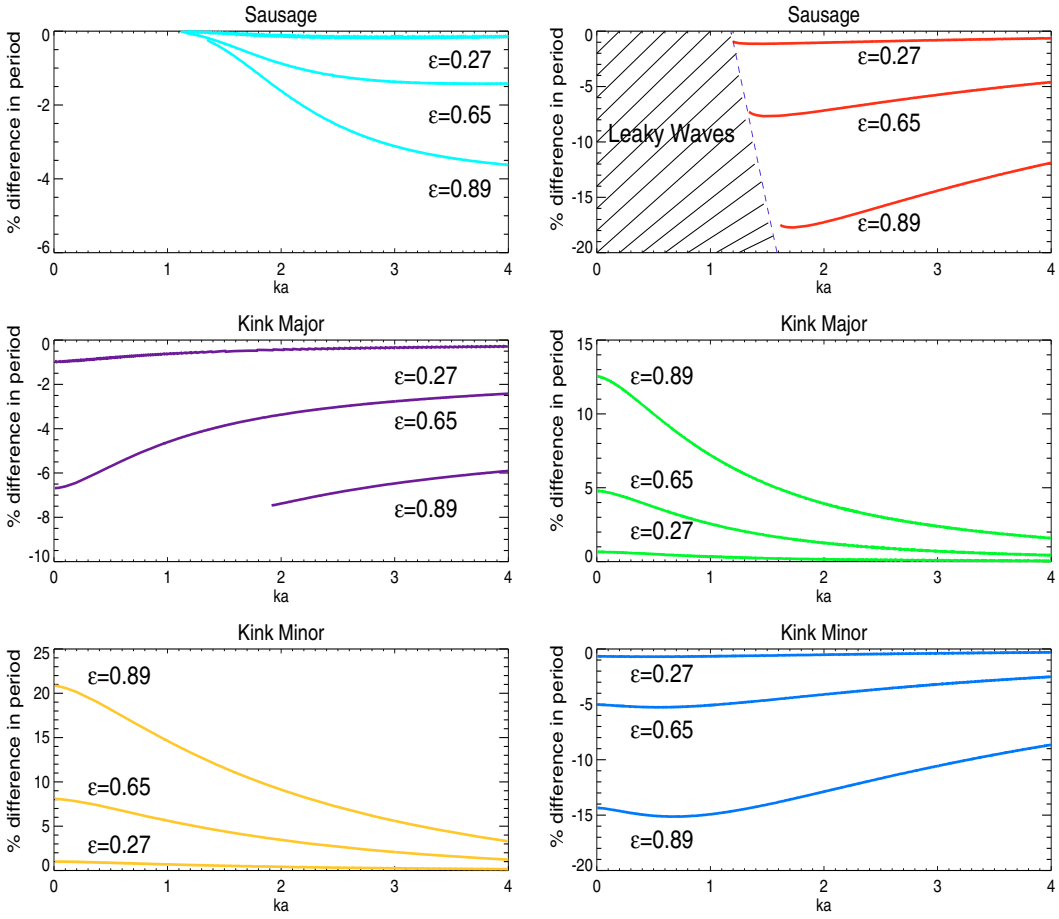

Fig. 6. Plotted is the percentage difference between the periods of the circular and elliptical cross sections against wavenumber for different values of ellipticity. The periods are of the fast waves. **a)** Shows difference in periods under typical photospheric conditions. **b)** Shows periods under coronal conditions.

in the thin tube approximation was also obtained. The propagation cutoff, k_c, for the fast sausage mode was also found in analogue to the cylindrical sausage cutoff and the cutoff value was found to increase with increasing ellipticity.

The tube was also found to support the slow and fast body kink modes and the slow and fast surface kink modes, of which only the fast mode was obtained by (Ruderman 2003). However, two kink frequencies $\omega_{1M,m}$ were found for each mode, i.e. each corresponding cylindrical mode splits into two. The kink mode with frequency ω_{1M} is polarised along the major axis and the kink mode with frequency ω_{1m} is polarised along the minor axis. The difference in the phase speeds between ω_{1M} and ω_{1m} is dependent on the ellipticity. The most profound effect can be seen when there is a large ellipticity (see Figs. 4b and 5b). However, as $\epsilon \to 0$, the difference between ω_{1M} and ω_{1m} becomes small. Figures 4a and 5a shows that for $\epsilon = 0.27$ (i.e. $s_0 = 2.0$) ω_{1M} and ω_{1m} have similar phase speeds and the dispersion diagrams look similar to the ones obtained by Edwin & Roberts (1983). In the limit of small ellipticity, the elliptical cross-section can then be approximated as a circle and the flux tube can be treated as a magnetic cylinder.

In addition, it was shown that there is a difference between the periods of the fast modes of an elliptical and a circular cross-section, see Fig. 6. The greater the ellipticity, the larger the difference between the periods of the two different geometries. The periods of the slow waves also differ between the elliptical and circular cross sections but was not shown explicitly.

However, the ellipticity is just one of many geometric and physical second-order effects (e.g. stratification, structuring, magnetic twist, curvature, wave leakage, variable background on the time scale of oscillations etc) that effect the period of a loop and whether the loop has an elliptical cross-section could not be determined from period alone. The level of difference in period could be very important in magneto-seismological applications, when observed periods are inverted into diagnostic properties (e.g. magnetic field strength, gravitational scale height, tube expansion parameter, ect.).

Furthermore, frequency ratios were calculated for the fast kink modes. Firstly, the ratio of ω_{1M} to ω_{1m} was found. Assuming that periods observed in coronal loops (Aschwanden et al. 1999) were associated with a loop with an ellipticity of 0.87, then the periods from the modes along the major and minor axis would differ by 80–115 s depending on orientation of the cross-section. The second ratio calculated was the ratio of the fundamental frequency to the first harmonic of the fast kink mode. Verwichte et al. (2004) observed multi-mode kink oscillations with frequency ratios of 1.64 and 1.81. The effect of ellipticity on this ratio was found to be far too small (i.e. $\ll 1$). It can be concluded the effects of ellipticity would be difficult to detect from observations of multi-modes.

With current spatial resolution, one would expect to observe an oscillation of the magnetic flux tube that would be a superposition of the oscillations polarised along the major axis and the minor axis. To find evidence of elliptical cross-sections, loop motions would need to resolved in the vertical and horizontal directions to obtain the two different periods. This may be possible with TRACE data (average cadence in EUV and UV wavelengths of 74 s) if the oscillations could be resolved in the horizontal and vertical directions or there could be a very high temporal resolution data set of kink oscillations available. It may be more likely that Solar Dynamic Observatory (SDO) observations will be the best candidate for the possible detection of elliptical cross-sections as the satellite will provide images with comparable resolution to TRACE and cadences of 10 s in EUV provided by the Atmospheric Imager Assembly.

Acknowledgements. The authors thank M. Ruderman, V. Fedun and G. Verth for a number of useful discussions. R.E. acknowledges M. Kéray for patient encouragement. R.M. acknowledges B. Carter for programming help. The authors are also grateful to NSF, Hungary (OTKA, Ref. No. K67746) and the Science and Technilogy Facilities Council (STFC), UK for the financial support they received.

Appendix A:

In this Appendix we fill in some of the steps required to obtain the general dispersion relations given by Eqs. (16)–(19). Relating the internal, Eq. (14), and external solutions, Eq. (15), by requiring that $\hat{v}_s$ and $P_{T,1}$ are continuous across the boundary s_0, gives

$$\frac{\left(\omega^2-\omega_i^2\right)}{2m_i^2}\left\{\alpha_0^i \mathrm{Ce}_0'\left(s_0,m_i^2\right)\mathrm{ce}_0\left(\varphi,m_i^2\right)\right.$$
$$\left.+\sum_{n=1}^{\infty}\left[\alpha_n^i \mathrm{Ce}_n'\left(s_0,m_i^2\right)\mathrm{ce}_n\left(\varphi,m_i^2\right)+\beta_n^i \mathrm{Se}_n'\left(s_0,m_i^2\right)\mathrm{se}_n\left(\varphi,m_i^2\right)\right]\right\}$$
$$=\frac{\left(\omega^2-\omega_e^2\right)}{2n_e^2}\left\{\alpha_0^e \mathrm{Fek}_0'\left(s_0,n_e^2\right)\mathrm{ce}_0\left(\varphi,n_e^2\right)\right.$$
$$+\sum_{n=1}^{\infty}\left[\alpha_n^e \mathrm{Fek}_n'\left(s_0,n_e^2\right)\mathrm{ce}_n\left(\varphi,n_e^2\right)\right.$$
$$\left.\left.+\beta_n^e \mathrm{Gek}_n'\left(s_0,n_e^2\right)\mathrm{se}_n\left(\varphi,n_e^2\right)\right]\right\} \quad (A.1)$$

and

$$\rho_i\left(c_i^2+v_{Ai}^2\right)\left(\omega_T^2-\omega^2\right)\left\{\alpha_0^i \mathrm{Ce}_0\left(s_0,m_i^2\right)\mathrm{ce}_0\left(\varphi,m_i^2\right)\right.$$
$$\left.+\sum_{n=1}^{\infty}\left[\alpha_n^i \mathrm{Ce}_n\left(s_0,m_i^2\right)\mathrm{ce}_n\left(\varphi,m_i^2\right)+\beta_n^i \mathrm{Se}_n\left(s_0,m_i^2\right)\mathrm{se}_n\left(\varphi,m_i^2\right)\right]\right\}$$
$$=\rho_e\left(c_e^2+v_{Ae}^2\right)\left(\omega_{Te}^2-\omega^2\right)\left\{\alpha_0^e \mathrm{Fek}_0\left(s_0,n_e^2\right)\mathrm{ce}_0\left(\varphi,n_e^2\right)\right.$$
$$+\sum_{n=1}^{\infty}\left[\alpha_n^e \mathrm{Fek}_n\left(s_0,n_e^2\right)\mathrm{ce}_n\left(\varphi,n_e^2\right)\right.$$
$$\left.\left.+\beta_n^e \mathrm{Gek}_n\left(s_0,n_e^2\right)\mathrm{se}_n\left(\varphi,n_e^2\right)\right]\right\}, \quad (A.2)$$

where the prime indicates the derivative with respect to s.

Expanding the Mathieu functions $\mathrm{ce}_n\left(\varphi,m_i^2\right)$ and $\mathrm{se}_n\left(\varphi,m_i^2\right)$ in Fourier series (Arscott 1964), we obtain

$$\mathrm{ce}_{2q+j}\left(\varphi,m_i^2\right)=\sum_{r=0}^{\infty}A_{2r+j}^{2q+j}\left(m_i^2\right)\cos[(2r+j)\varphi] \quad (A.3)$$

$$\mathrm{se}_{2q+1+j}\left(\varphi,m_i^2\right)=\sum_{r=0}^{\infty}B_{2r+1+j}^{2q+1+j}\left(m_i^2\right)\sin[(2r+1+j)\varphi] \quad (A.4)$$

where $q = 0, 1, 2...$ and $j = 0, 1$. The coefficients $A_{2r+j}^{2q+j}\left(m_i^2\right)$ and $B_{2r+1+j}^{2q+1+j}(n_i^2)$ are related by recurrence relations which can be found in Abramowitz & Stegun (1964). These expansions can be substituted into Eqs. (A.1) and (A.2) to give Eqs. (16)–(19).

Taking the cold plasma case ($c_i = c_e = 0$), then $m_i^2 = \sigma^2\left(\omega^2-\omega_{Ai}^2\right)/4v_{Ai}^2$, $m_e^2 = \sigma^2\left(\omega^2-\omega_{Ae}^2\right)/4v_{Ae}^2$ and Eqs. (16)-(19) reduce to

$$m_i^{-2}\sum_{q=0}^{\infty}\alpha_{2q+j}^i \mathrm{Ce}_{2q+j}'\left(s_0,m_i^2\right)A_{2r+j}^{2q+j}\left(m_i^2\right)=$$
$$-n_e^{-2}\sum_{q=0}^{\infty}\alpha_{2q+j}^e \mathrm{Fek}_{2q+j}'\left(s_0,n_e^2\right)A_{2r+j}^{2q+j}\left(n_e^2\right) \quad (A.5)$$

$$\rho_i v_{Ai}^2\omega^2\sum_{q=0}^{\infty}\alpha_{2q+j}^i \mathrm{Ce}_{2q+j}\left(s_0,m_i^2\right)A_{2r+j}^{2q+j}\left(m_i^2\right)=$$
$$\rho_e v_{Ae}^2\omega^2\sum_{q=0}^{\infty}\alpha_{2q+j}^e \mathrm{Fek}_{2q+j}\left(s_0,n_e^2\right)A_{2r+j}^{2q+j}\left(n_e^2\right) \quad (A.6)$$

and

$$m_i^{-2}\sum_{q=0}^{\infty}\beta_{2q+1+j}^i \mathrm{Se}_{2q+1+j}'\left(s_0,m_i^2\right)B_{2r+1+j}^{2q+1+j}\left(m_i^2\right)=$$
$$-n_e^{-2}\sum_{q=0}^{\infty}\beta_{2q+1+j}^e \mathrm{Gek}_{2q+1+j}'\left(s_0,n_e^2\right)B_{2r+1+j}^{2q+1+j}\left(n_e^2\right) \quad (A.7)$$

$$\rho_i v_{Ai}^2\omega^2\sum_{q=0}^{\infty}\beta_{2q+1+j}^i \mathrm{Se}_{2q+1+j}\left(s_0,m_i^2\right)B_{2r+1+j}^{2q+1+j}\left(m_i^2\right)=$$
$$\rho_e v_{Ae}^2\omega^2\sum_{q=0}^{\infty}\beta_{2q+1+j}^e \mathrm{Gek}_{2q+1+j}\left(s_0,n_e^2\right)B_{2r+1+j}^{2q+1+j}\left(n_e^2\right) \quad (A.8)$$

which are the equations found by Ruderman (2003).

Appendix B:

In this appendix is a list of the modified Mathieu functions with there expansions in terms of Bessel functions (Bateman 1955; McLachlan 1947). The following expressions are valid for $m_i^2 < 0$ (body waves):

$$\mathrm{Ce}_{2m}(s,m_i^2)=\frac{u_{2m}}{A_0^{2m}}\sum_{r=0}^{\infty}(-1)^r A_{2r}^{2m}\left[J_r(|m_i|e^s)J_r(|m_i|e^{-s})\right] \quad (B.1)$$

$$\mathrm{Ce}_{2m+1}(s,m_i^2)=\frac{u_{2m+1}}{A_1^{2m+1}}\sum_{r=0}^{\infty}(-1)^r A_{2r+1}^{2m+1}$$
$$\times\left[J_r(m_i e^{-s})J_{r+1}(m_i e^s)+J_{r+1}(m_i e^{-s})J_r(m_i e^s)\right] \quad (B.2)$$

$$\mathrm{Se}_{2m+1}(s,m_i^2)=i\frac{q_{2m+1}}{B_1^{2m+1}}\sum_{r=0}^{\infty}(-1)^r B_{2r+1}^{2m+1}$$
$$\times[J_r(m_i e^{-s})J_{r+1}(m_i e^s)-J_{r+1}(m_i e^{-s})J_r(m_i e^s)]. \quad (B.3)$$

The expansion of the Mathieu functions in terms of Bessel functions for n_i^2 (surface waves) are, from McLachlan (1947),

$$\mathrm{Ce}_{2m}(s,m_i^2) = \frac{u_{2m}}{A_0^{2m}}\sum_{r=0}^{\infty} A_{2r}^{2m}[I_r(n_i e^s)I_r(n_i e^{-s})], \tag{B.4}$$

$$\mathrm{Ce}_{2m+1}(s,m_i^2) = i\frac{u_{2m+1}}{A_1^{2m+1}}\sum_{r=0}^{\infty} A_{2r+1}^{2m+1} \times\left[I_r(n_i e^{-s})J_{r+1}(n_i e^{s})+I_{r+1}(n_i e^{-s})I_r(n_i e^{s})\right], \tag{B.5}$$

$$\mathrm{Se}_{2m+1}(s,m_i^2) = \frac{q_{2m+1}}{B_1^{2m+1}}\sum_{r=0}^{\infty} B_{2r+1}^{2m+1} \times\left[I_r(n_i e^{-s})I_{r+1}(n_i e^{s}) - I_{r+1}(n_i e^{-s})I_r(n_i e^{s})\right], \tag{B.6}$$

$$\mathrm{Se}_{2m+2}(s,m_i^2) = \frac{q_{2m+2}}{B_1^{2m+2}}\sum_{r=0}^{\infty} B_{2r+2}^{2m+2} \times\left[I_r(n_i e^{-s})I_{r+2}(n_i e^{s}) - I_{r+2}(n_i e^{-s})I_r(n_i e^{s})\right], \tag{B.7}$$

where $m_i^2 = -n_i^2 < 0$.

Approximation of Mathieu functions of the third kind valid for $m_e^2 < 0$:

$$\mathrm{Fek}_{2m+1}(s,n_e^2) = \frac{u_{2m+1}}{\pi A_1^{2m+1}}\sum_{r=0}^{\infty}(-1)^r A_{2r+1}^{2m+1} \times[I_r(n_e e^{-s})K_{r+1}(n_e e^{s}) - I_{r+1}(n_e e^{-s})K_r(n_e e^{s})], \tag{B.8}$$

$$\mathrm{Gek}_{2m+1}(s,n_e^2) = \frac{q_{2m+1}}{\pi B_1^{2m+1}}\sum_{r=0}^{\infty}(-1)^r B_{2r+1}^{2m+1} \times([I_r(n_e e^{-s})K_{r+1}(n_e e^{s}) + I_{r+1}(n_e e^{-s})K_r(n_e e^{s})]. \tag{B.9}$$

The following equations are (B.1), (B.2), (B.3) differentiated with respect to s for particular values of n and are also valid for $m_i^2 < 0$:

$$\mathrm{Ce}_0'(s,m_i^2) \sim -m_i\Big[J_0(|m_i|e^{-s})e^s J_1(|m_i|e^s) - J_0(|m_i|e^s)e^{-s}J_1(|m_i|e^{-s})\Big]. \tag{B.10}$$

$$\mathrm{Ce}_1'(s,m_i^2) \sim m_i\Big\{[J_1(|m_i|e^{-s})J_1(|m_i|e^s)]e^{-s} + [J_0(|m_i|e^s) -\frac{e^{-s}}{|m_i|}J_1(|m_i|e^s)]e^s J_0(|m_i|e^{-s}) - [J_0(|m_i|e^{-s}) -\frac{e^s}{|m_i|}J_1(|m_i|e^{-s})]e^{-s}J_0(|m_i|e^s) - e^s J_1(|m_i|e^{-s})J_1(|m_i|e^s)\Big\} \tag{B.11}$$

$$\mathrm{Se}_1'(s,m_i^2) \sim |m_i|\Big\{[J_1(|m_i|e^{-s})J_1(|m_i|e^s)]e^{-s} + [J_0(|m_i|e^s) -\frac{e^{-s}}{|m_i|}J_1(|m_i^2|e^s)]e^s J_0(|m_i|e^{-s}) + [J_0(|m_i|e^{-s}) -\frac{e^s}{|m_i|}J_1(|m_i|e^{-s})]e^{-s}J_0(|m_i|e^s) +e^s J_1(|m_i|e^{-s})J_1(|m_i|e^s)\Big\} \tag{B.12}$$

Appendix C:

The expansions of the Mathieu functions of the third kind valid for $|m_e|e^s \ll 1$ have been found by Ruderman (2003) and can be written:

$$\mathrm{Fek}_0(s,n_e^2) \sim -u_0(\ln|n_e| + 2s + 2\gamma - 2\ln 2),$$

$$\mathrm{Fek}_{2r+1}(s,n_e^2) \sim \frac{(-1)^r u_{2r+1}}{\pi|n_e|A_1^{2r+1}}e^{-(2r+1)s},$$

$$\mathrm{Fek}_{2r+2}(s,n_e^2) \sim \frac{(-1)^r u_{2r+2}}{\pi(2r+2)A_1^{2r+2}}e^{-(2r+2)s},$$

$$\mathrm{Gek}_{2r+1}(s,n_e^2) \sim \frac{(-1)^r q_{2r+1}}{\pi|n_e|B_1^{2r+1}}e^{-(2r+1)s},$$

$$\mathrm{Gek}_{2r+2}(s,n_e^2) \sim \frac{(2r+2)(-1)^r q_{2r+2}}{\pi n_e^2 B_1^{2r+2}}e^{-(2r)s}.$$

Appendix D:

In this Appendix, we describe the method for finding the perturbations of the focal points of the elliptical cross-section. From the set of Eqs. (12), we have expressions for $\hat{v}_s$ and $\hat{v}_\varphi$ in terms of $\hat{\Delta} = S(s)\Phi(\varphi)$ which for $\hat{\Delta} = \mathrm{Ce}_n(s,m_i^2)\mathrm{ce}_n\left(\varphi,m_i^2\right)$ gives

$$\hat{v}_s(s,\varphi) = n\left(A_n^n\left(m_i^2\right)\right)^2\frac{\left(\omega_i^2-\omega^2\right)}{\sigma\omega^2 m_i^2}\cos n\varphi \times\frac{\sinh(ns)}{\sinh(s)}\left(1+\frac{\sin^2(\varphi)}{\sinh^2(s)}\right)^{-1/2}, \tag{D.1}$$

$$\hat{v}_\varphi(s,\varphi) = -n\left(A_n^n\left(m_i^2\right)\right)^2\frac{\left(\omega_i^2-\omega^2\right)}{\sigma\omega^2 m_i^2}\cosh(ns) \times\frac{\sin(n\varphi)}{\sin(\varphi)}\left(1+\frac{\sinh^2(s)}{\sin^2(\varphi)}\right)^{-1/2}, \tag{D.2}$$

where $n \geq 0$ (i.e. for even Mathieu functions) and for $\hat{\Delta} = Se_n(s,m_i^2)se_n\left(\varphi,m_i^2\right)$,

$$\hat{v}_s(s,\varphi) = n\left(B_n^n\left(m_i^2\right)\right)^2\frac{\left(\omega_i^2-\omega^2\right)}{\sigma\omega^2 m_i^2}\cosh(ns) \times\frac{\sin(n\varphi)}{\sin(\varphi)}\left(1+\frac{\sinh^2(s)}{\sin^2(\varphi)}\right)^{-1/2}, \tag{D.3}$$

$$\hat{v}_\varphi(s,\varphi) = n\left(B_n^n\left(m_i^2\right)\right)^2\frac{\left(\omega_i^2-\omega^2\right)}{\sigma\omega^2 m_i^2}\cos n\varphi \times\frac{\sinh(ns)}{\sinh(s)}\left(1+\frac{\sin^2(\varphi)}{\sinh^2(s)}\right)^{-1/2}, \tag{D.4}$$

where $n > 0$ (i.e. for odd Mathieu functions). The focal points have coordinates $(s,\varphi) = (0,0)$ and $(0,\pi)$ and it is clear to see from Eqs. (D.1) and (D.2) that for the sausage mode ($n = 0$)

$$\hat{v}_s = 0, \qquad \hat{v}_\varphi = 0$$

for $(0,0)$ and $(0,\pi)$, hence the focal points do *not* move for the sausage mode. When $n>0$, the perturbations at the focal points for Eqs. (D.1) and (D.2) are

$$\hat{v}_{\rm s}(0,0)=n\left(A_n^n\left(m_{\rm i}^2\right)\right)^2\frac{\left(\omega_{\rm i}^2-\omega^2\right)}{\sqrt{2\sigma\omega^2m_{\rm i}^2}},$$

$$\hat{v}_{\varphi}(0,0)=-n\left(A_n^n\left(m_{\rm i}^2\right)\right)^2\frac{\left(\omega_{\rm i}^2-\omega^2\right)}{\sqrt{2\sigma\omega^2m_{\rm i}^2}},$$

and

$$\hat{v}_{\rm s}(0,\pi)=n\left(A_n^n\left(m_{\rm i}^2\right)\right)^2\frac{\left(\omega_{\rm i}^2-\omega^2\right)}{\sqrt{2\sigma\omega^2m_{\rm i}^2}}\cos n\pi,$$

$$\hat{v}_{\varphi}(0,\pi)=-n\left(A_n^n\left(m_{\rm i}^2\right)\right)^2\frac{\left(\omega_{\rm i}^2-\omega^2\right)}{\sqrt{2\sigma\omega^2m_{\rm i}^2}}.$$

From Eqs. (D.3) and (D.4) the perturbations at the focal points for $n>0$ are

$$\hat{v}_{\rm s}(0,0)=n\left(B_n^n\left(m_{\rm i}^2\right)\right)^2\frac{\left(\omega_{\rm i}^2-\omega^2\right)}{\sqrt{2\sigma\omega^2m_{\rm i}^2}},$$

$$\hat{v}_{\varphi}(0,0)=\left(B_n^n\left(m_{\rm i}^2\right)\right)^2\frac{\left(\omega_{\rm i}^2-\omega^2\right)}{\sqrt{2\sigma\omega^2m_{\rm i}^2}},$$

and

$$\hat{v}_{\rm s}(0,\pi)=n\left(B_n^n\left(m_{\rm i}^2\right)\right)^2\frac{\left(\omega_{\rm i}^2-\omega^2\right)}{\sqrt{2\sigma\omega^2m_{\rm i}^2}},$$

$$\hat{v}_{\varphi}(0,\pi)=n\left(B_n^n\left(m_{\rm i}^2\right)\right)^2\frac{\left(\omega_{\rm i}^2-\omega^2\right)}{\sqrt{2\sigma\omega^2m_{\rm i}^2}}\cos n\pi.$$

Using the relationships between unit vectors of the elliptic, $\boldsymbol{e}_{\rm s}$ and $\boldsymbol{e}_{\varphi}$, and Cartesian coordinates, $\boldsymbol{e}_x$ and $\boldsymbol{e}_y$,

$$\boldsymbol{e}_x=H^{-1}(\boldsymbol{e}_{\rm s}\sinh s\cos\varphi-\boldsymbol{e}_{\varphi}\cosh s\sin\varphi),$$

$$\boldsymbol{e}_y=H^{-1}(\boldsymbol{e}_{\rm s}\cosh s\sin\varphi+\boldsymbol{e}_{\varphi}\sinh s\cos\varphi),$$

the velocity perturbations v_x and v_y can be found.

References

Abramowitz, M., & Stegun, I. 1964, Handbook of Mathematical Functions (National Bureau of Standards)
Andries, J., Arregui, I., & Goossens, M. 2005a, ApJ, 624, L57
Andries, J., Goossens, M., Hollweg, J. V., Arregui, I., & Van Doorsselaere, T. 2005b, A&A, 430, 1109
Arscott, F. 1964, International Series of Monographs in Pure and Applied Mathematics, Vol. 66, Periodic Differential Equations (Pergamon Press)
Aschwanden, M. J. 2005, Physics of the Solar Corona. An Introduction with Problems and Solutions, 2nd edn. (Pour la Science)
Aschwanden, M. J., Fletcher, L., Schrijver, C. J., & Alexander, D. 1999, ApJ, 520, 880
Banerjee, D., Erdélyi, R., Oliver, R., & O'Shea, E. 2007, Sol. Phys., 246, 3
Bateman, H. 1955, Higher transcendental functions, California Institute of Technology Bateman Manuscript Project (New York: McGraw-Hill), 1953–1955
Bennett, K., Roberts, B., & Narain, U. 1999, Sol. Phys., 185, 41
Cally, P. S. 1986, Sol. Phys., 103, 277
De Pontieu, B., Martens, P. C. H., & Hudson, H. S. 2001, ApJ, 558, 859
Díaz, A. J., & Roberts, B. 2006, A&A, 458, 975
Díaz, A. J., Donnelly, G. R., & Roberts, B. 2007, A&A, 476, 359
Donnelly, G. R., Díaz, A. J., & Roberts, B. 2006, A&A, 457, 707
Dymova, M. V., & Ruderman, M. S. 2006, A&A, 457, 1059
Edwin, P. M., & Roberts, B. 1982, Sol. Phys., 76, 239
Edwin, P. M., & Roberts, B. 1983, Sol. Phys., 88, 179
Erdélyi, R., & Carter, B. K. 2006, A&A, 455, 361
Erdélyi, R., & Fedun, V. 2006, Sol. Phys., 238, 41
Erdélyi, R., & Verth, G. 2007, A&A, 462, 743
Gutiérrez-Vega, J. C., Rodríguez-Dagnino, R. M., Meneses-Nava, M. A., & Chávez-Cerda, S. 2003, American J. Phys., 71, 233
Karami, K., Nasiri, S., & Sobouti, Y. 2002, A&A, 396, 993
Korn, G., & Korn, T. 1961, Mathematical Handbook for Scientists and Engineers (New York: McGraw-Hill)
Lighthill, M. J. 1960, Phil. Trans. Roy. Soc. A, 252, 397
McEwan, M. P., Donnelly, G. R., Díaz, A. J., & Roberts, B. 2006, A&A, 460, 893
McLachlan, N. 1947, Theory and Application of Mathieu Functions (Oxford: Oxford University Press)
Mendoza-Briceño, C. A., Erdélyi, R., & Sigalotti, L. D. G. 2004, ApJ, 605, 493
Roberts, B. 1981, Sol. Phys., 69, 27
Roberts, B. 2000, Sol. Phys., 193, 139
Roberts, B., Edwin, P. M., & Benz, A. O. 1984, ApJ, 279, 857
Roberts, B. & Webb, A. R. 1978, Sol. Phys., 56, 5
Roberts, B., & Webb, A. R. 1979, Sol. Phys., 64, 77
Ruderman, M. S. 2003, A&A, 409, 287
Ruderman, M. S. 2005, in The Dynamic Sun: Challenges for Theory and Observations, ESA-SP, 600
Ruderman, M. S. 2007, Sol. Phys., 246, 119
Ruderman, M. S., & Roberts, B. 2002, ApJ, 577, 475
Ruderman, M. S., & Roberts, B. 2005, J. Plasma Phys., 72, 285
Spruit, H. C. 1982, Sol. Phys., 75, 3
Van Doorsselaere, T., Debosscher, A., Andries, J., & Poedts, S. 2004, A&A, 424, 1065
Verth, G., van Doorsselaere, T., Erdélyi, R., & Goossens, M. 2007, A&A, 475, 341
Verwichte, E., Nakariakov, V. M., Ofman, L., & Deluca, E. E. 2004, Sol. Phys., 223, 77